JGR Atmospheres

RESEARCH ARTICLE
10.1029/2024JD041740

# How Well Do AMIP6 and CMIP6 Reproduce the Specific Extreme El Niño Teleconnections to North America?

**Margot Beniche[1], Jérôme Vialard[2], Matthieu Lengaigne[3], and Nicholas M. J. Hall[1]**

[1]LEGOS, CNRS/CNES/IRD/Université de Toulouse, Toulouse, France, [2]LOCEAN-IPSL, IRD/CNRS/MNHN/Sorbonne Université, Paris, France, [3]MARBEC, IRD/IFREMER/CNRS/Université de Montpellier, Sète, France

**Key Points:**

- In 22/23 AMIP6 ensemble simulations, the North American ENSO teleconnection pattern only shifts eastward during extreme El Niño events
- The extreme El Niño teleconnection pattern and its impacts (warm Northeast America, wet California and Florida) are very reproducible
- Most CMIP6 models that produce extreme El Niño events reproduce their teleconnection pattern, but downplay wet California/Florida anomalies

**Supporting Information:**

Supporting Information may be found in the online version of this article.

**Correspondence to:**

M. Beniche,
margot.beniche@univ-tlse3.fr

**Citation:**

Beniche, M., Vialard, J., Lengaigne, M., & Hall, N. M. J. (2025). How well do AMIP6 and CMIP6 reproduce the specific extreme El Niño teleconnections to North America? *Journal of Geophysical Research: Atmospheres*, *130*, e2024JD041740. https://doi.org/10.1029/2024JD041740

Received 5 JUN 2024
Accepted 13 JAN 2025

**Author Contributions:**

**Conceptualization:** Jérôme Vialard, Matthieu Lengaigne
**Data curation:** Margot Beniche
**Formal analysis:** Margot Beniche, Jérôme Vialard, Matthieu Lengaigne
**Funding acquisition:** Jérôme Vialard, Nicholas M. J. Hall
**Methodology:** Matthieu Lengaigne
**Supervision:** Nicholas M. J. Hall
**Writing – original draft:** Margot Beniche
**Writing – review & editing:** Jérôme Vialard, Matthieu Lengaigne



**Abstract** Extreme El Niño events (e.g., 1982–1983, 1997–1998) are characterized by strong, eastward-shifted warm Sea Surface Temperature anomalies, and a southward migration of the eastern Pacific Inter-Tropical Convergence Zone (ITCZ) to the equator. Using an ensemble simulation with a single AMIP6 model, Beniche et al. (2024, https://doi.org/10.1038/s41598-024-52580-9) suggested that such events uniquely yield an eastward shift of the Pacific-North American (PNA) teleconnection pattern, with specific impacts over North America. Here, we first examine the robustness of these results in 135 ensemble members from 23 different AMIP6 models. The specific, eastward-shifted extreme El Niño teleconnection pattern is robust in all models but one. It is also highly reproducible across years and ensemble members, due to stronger teleconnection amplitude than that of internal atmospheric noise. This yields specific, predictable impacts (defined as $> 0.5$ STD) such as warm conditions over Northeast America (69% chances), and wet anomalies over California (77%) and Florida (97%). We then show that 26 out of the 42 CMIP6 models we examined reproduce extreme El Niño events, defined as El Niño events associated with large eastern Pacific rainfall anomalies. These models tend to have a weaker cold tongue bias than the rest of CMIP6. Despite a degradation in performance from AMIP6 to CMIP6, 18 out of the 26 selected models capture the specific extreme El Niño teleconnections, albeit with some underestimation of wet anomalies over California and Florida. We end by discussing implications for future North American climate projections based on CMIP6.

**Plain Language Summary** The El Niño-Southern Oscillation (ENSO) alternates between a warm and wet (El Niño) or cold and dry (La Niña) central-eastern equatorial Pacific. ENSO events modify the atmospheric circulation, leading to climate impacts over remote regions, including North America. This is known as ENSO teleconnections. Occasionally, El Niño escalates into extreme events, characterized by strong and eastward-shifted equatorial Pacific warm anomalies compared to weaker events. By analyzing a large database of atmospheric models forced by observed Sea Surface Temperature, we demonstrate that these extreme El Niño events produce North American teleconnection pattern and impacts that are distinct from those of milder events, and more reproducible. Extreme El Niño in particular results in high probability of warm anomalies over Northeast America and wet anomalies over California and Florida. Not all coupled ocean-atmosphere climate models can simulate extreme El Niño events, but most of those that do reproduce their specific teleconnection pattern, albeit with underestimations of wet conditions over California and Florida. We discuss the implications of our results for future projections of the North American climate.

## 1. Introduction

The El Niño-Southern Oscillation (ENSO) is the primary driver of interannual climate variability (e.g., McPhaden et al., 2006; Taschetto et al., 2020; Timmermann et al., 2018). El Niño-Southern Oscillation is characterized by alternating warm (El Niño) and cold (La Niña) Sea Surface Temperature (SST) anomalies in the central and eastern equatorial Pacific. These anomalies trigger changes in tropical atmospheric convection, setting off extratropical atmospheric responses known as teleconnections (Horel & Wallace, 1981; Hoskins & Karoly, 1981). With ENSO predictability extending several seasons in advance (L'Heureux et al., 2020), those teleconnections are crucial in accurately forecasting seasonal rainfall and surface temperature across North America during boreal winter (J. Yu et al., 2012; Kumar & Hoerling, 1995, 1998). El Niño-Southern Oscillation teleconnections are mostly associated with the Pacific-North American (PNA) pattern (Horel & Wallace, 1981; Wallace & Gutzler, 1981), whose positive (negative) phase is associated with El Niño (La Niña) events (Livezey & Mo, 1987). The PNA features centers of action over the Aleutian Islands and western Canada, facilitating the northward advection of warmer air over Northwest US and Canada (Ropelewski & Halpert, 1986).

**Table 1**
*List of the 23 AMIP6 Models With at Least 3 Ensemble Members Available, Analyzed Over the Period 1979–2014*

| Model | M members | Variant |
|---|---|---|
| ACCESS-CM2 | 4 | f1 |
| ACCESS-ESM1-5 | 10 | f1 |
| BCC-CSM2-MR | 3 | f1 |
| BCC-ESM1 | 3 | f1 |
| CAMS-CSM1-0 | 3 | f1 |
| CAS-ESM2-0 | 4 | f1 |
| CESM2 | 10 | f1 |
| CESM2-FV2 | 3 | f1 |
| CESM2-WACCM | 3 | f1 |
| CNRM-CM6-1 | 16 | f2 |
| E3SM-1-0 | 3 | f1 |
| E3SM-2-0 | 3 | f1 |
| FGOALS-f3-L | 3 | f1 |
| GISS-E2-1-G | 5 | f1 |
| IPSL-CM6A-LR | 22 | f1 |
| MIROC6 | 10 | f1 |
| MIROC-ES2L | 3 | f2 |
| MPI-ESM-1-2-HAM | 3 | f1 |
| MPI-ESM1-2-HR | 3 | f1 |
| MPI-ESM1-2-LR | 3 | f1 |
| MRI-ESM2-0 | 3 | f1 |
| NESM3 | 5 | f1 |
| NorCPM1 | 10 | f1 |
| Total members | 135 | |

*Note.* The center column indicates the number of members *M*, and the left column indicates the forcing variant of the model.

El Niño-Southern Oscillation is also linked to another teleconnection pattern known as the Tropical-Northern Hemisphere (TNH) pattern (Livezey & Mo, 1987; Mo & Livezey, 1986), which exhibits an eastward shift and a phase quadrature relative to the PNA pattern (Barnston & Livezey, 1987). Early studies suggested that the nonlinear response of the tropical convection to SST resulted in eastward-shifted rainfall anomalies during El Niño relative to La Niña, triggering the TNH pattern (Hoerling et al., 1997; Peng & Kumar, 2005). El Niño-Southern Oscillation diversity (Capotondi et al., 2015) distinguishes El Niño events with peak SST anomalies in the Central Pacific (CP, Dateline or Modoki) and Eastern Pacific (EP) events (Ashok et al., 2007; Kug et al., 2009; Takahashi et al., 2011). Hoerling and Kumar (2002); J. Yu et al. (2012); B. Yu et al. (2015) suggested that only EP events trigger the TNH teleconnection and associated impacts (Feng et al., 2016; Mo, 2010), whereas Chiodi and Harrison (2013); Chiodi and Harrison (2015); Johnson and Kosaka (2016) pointed out the necessity of deep convective anomalies over the central-eastern Pacific to induce impacts over North America, noting that only sufficiently large EP events could trigger anomalies over this climatological cold region.

Some El Niño events, such as in 1982–1983 and 1997–1998, produce very large eastern Pacific SST and rainfall anomalies (Cai et al., 2014), leading to classify them as extreme El Niño events. These extreme Niño events play a pivotal role in shaping the SST and rainfall asymmetry between El Niño and La Niña (Bayr et al., 2024; Liu et al., 2024; Srinivas et al., 2024). Their large SST anomalies exceed the convective threshold over the eastern Pacific, inducing large eastern Pacific rainfall anomalies (Bayr et al., 2024; Srinivas et al., 2024). Consequently, extreme El Niño events are found to drive more systematic wet anomalies over California (J. Lee et al., 2023; S. Lee et al., 2018; Hoell et al., 2016). Building on these studies, Beniche et al. (2024) used Atmospheric General Circulation model (AGCM) experiments to demonstrate that such extreme El Niño events are the sole contributor to the diversity of winter ENSO teleconnections over North America. In other words, they demonstrate that while both La Niña and moderate El Niño events (EP and CP alike) induce a PNA response (positive for El Niño, and negative for La Niña), only extreme El Niño events can trigger a TNH response and wet anomalies over the western US coast.

However, Beniche et al. (2024) only considered a single 16-members ensemble with the CNRM-CM6.1 atmospheric component (Roehrig et al., 2020), whereas 55 atmospheric models simulations forced by observed SST and sea-ice are available in the Atmospheric model Intercomparison Project (AMIP) database. AGCM suffer from various biases, attributable to imperfect parameterizations (Xiang et al., 2017; Zhang et al., 2024), raising doubts about the robustness of the teleconnection patterns derived from a single model. Second, extratropical atmospheric internal variability is substantial (Kumar & Hoerling, 1995), and the PNA pattern displays intrinsic fluctuations (Straus & Shukla, 2000, 2002) in addition to the SST-forced ones. This large internal noise can obscure the ENSO-driven signal, leading to large sampling errors on ENSO teleconnections patterns in both observations (Garfinkel et al., 2012) and models (O'Reilly, 2018; Sardeshmukh et al., 2000). Addressing this issue requires large sample sizes (Deser et al., 2018; Garfinkel et al., 2018), which can be achieved from large ensemble simulations. The first objective of this study is therefore to ascertain the robustness of Beniche et al. (2024) results using a broader database (see Table 1), encompassing a total of 135 ensemble members from 23 different AMIP6 models over 1979–2014. This approach will both address the sampling issue, and assess robustness of the Beniche et al. (2024) results in other AGCMs (note, however, that unlike Beniche et al. (2024), the present study only includes the 1982 and 1997 extreme El Niño events because most AMIP6 simulations end in 2014). Beniche et al. (2024) emphasized that the extreme El Niño teleconnections and impacts over North America were much more reproducible compared to those of moderate El Niño or La Niña events. Therefore, our second objective is to investigate the extreme El Niño teleconnection reproducibility within the extensive AMIP6

database and explore whether this reproducibility arises from large-amplitude of the teleconnection response during extreme El Niño (in other words, stronger signal) or from reduced internal atmospheric variability during such events (in other words, weaker noise).

Finally, projections from the Coupled Model Intercomparison Project (CMIP) database, particularly CMIP6 (Eyring et al., 2016), indicate an increase in extreme El Niño frequency (Cai et al., 2021; Heede & Fedorov, 2023b) and larger El Niño EP events (Shin et al., 2022) in warmer climates. The results of Beniche et al. (2024) consequently imply more frequent ENSO impacts over North America in a warmer climate. Coupled Model Intercomparison Project models, however, are known to suffer from large systematic biases that can affect their representation of ENSO teleconnections. Notably, CMIP models display a persistent "cold tongue" bias in the equatorial Pacific SST climatology, associated with a dry equatorial bias, which has been observed across multiple CMIP generations (Bellenger et al., 2013; Planton et al., 2021). This SST bias can prevent the initiation of deep convection, even in the presence of large, eastward-shifted SST anomalies characteristic of extreme El Niño events, potentially preventing the occurrence of large eastern Pacific rainfall anomalies (Cai et al., 2014) that trigger the TNH response (Beniche et al., 2024). Additionally, CMIP atmospheric mean state biases can affect the Rossby wave pattern that underpins teleconnections to the Pacific-North American sector (Li et al., 2020). These systematic biases may compromise the CMIP6 model's ability to accurately reproduce the distinctive TNH-like teleconnection pattern associated with extreme El Niño in the present climate. Therefore, our third objective is to investigate whether CMIP6 models can reproduce the specific teleconnection pattern of extreme El Niño diagnosed from the AMIP6 simulations.

This paper is organized as follows. Section 2 present our observational, AMIP6 and CMIP6 data sets and methods. In Section 3, we demonstrate that the specific extreme El Niño teleconnection pattern discussed by Beniche et al. (2024) is robust and across 22 out of 23 examined AMIP simulations, and investigate the cause of its strong reproducibility. In Section 4, we assess the performance of CMIP6 models in simulating extreme El Niño events, with 26 out of 42 models which are able to simulate strong eastern Pacific rainfall anomalies during such events. These models reproduce the AMIP6 extreme El Niño teleconnection pattern reasonably well, despite an underestimation of extreme El Niño wet anomalies over California and Florida. In Section 5, we summarize our results, and discuss them with an emphasis on perspectives regarding the use of CMIP6 models to investigate future ENSO teleconnections over North America.

## 2. Methods and Data

We implement a standardized data processing methodology to ensure consistency across all data sets. Monthly values are first linearly detrended and then averaged over the boreal winter season (December-January-February, DJF), aligning with the peak activity periods of both ENSO-related tropical SST anomalies and the PNA/TNH teleconnections patterns (Barnston & Livezey, 1987; Rasmusson & Carpenter, 1982). Anomalies are computed relatively to a 1979–2014 DJF climatology for AMIP6 and observed data sets, and 1850–2014 DJF for CMIP6. All data sets are bi-linearly interpolated to a standard $1° \times 1°$ grid. Normalized composites refer to composites built from individual years divided by the DJF average N3.4 SST anomaly. When no mention of normalization is made, a classical composite is displayed.

We use Hadley Center Sea Ice and Sea Surface Temperature (HadISST) SST (Rayner, 2003), Global Precipitation Climatology Project v2.3 rainfall (Adler et al., 2018) and ERA5 reanalysis (Hersbach et al., 2020) 2-m height Temperature (T2m) and 500-hPa geopotential height.

We consider 23 AMIP6 models (see Table 1), selecting models with a minimum of 3 ensemble-members covering the 1979–2014 period. Some modeling centers provide several AMIP simulations, based on different versions of the same core model, so that those 23 simulations are based on 16 core models. Most centers have only provided AMIP6 simulations over the recommended 1979–2014 period (Eyring et al., 2016), with only four models providing extended simulations that cover the 2015/2016 extreme El Niño event. That would only have provided 15 additional members for that event to those already analyzed by Beniche et al. (2024). To ensure a consistent number of members for each ENSO event, we therefore chose not to include the 2015/2016 extreme El Niño event. The variants selected are "i1p1f1", except for the AMIP6.CNRM-CM6.1 and AMIP6.MIROC-ES2L models, which are "i1p1f2". Forcing SSTs are prescribed based on observations (Eyring et al., 2016). Prior to computing the composites of multi-model ensemble mean (MMEM), ensemble-means (EMs) for individual

**Table 2**
*List of the 42 CMIP6 First Variants Used (One Member Per Model) Considered for the Analysis Over 1850–2014*

| CMIP6 model first variant | (r1i1p1f1 or r2i1p1f2) |
|---|---|
| ACCESS-CM2 [a,b] | HadGEM3-GC31-LL |
| ACCESS-ESM1-5 | HadGEM3-GC31-MM [a] |
| BCC-CSM2-MR | INM-CM4-8 |
| BCC-ESM1 | INM-CM5-0 |
| CAMS-CSM1-0 [a,b] | IPSL-CM6A-LR |
| CanESM5 | KACE-1-0-G [a] |
| CESM2 [a,b] | KIOST-ESM [a] |
| CESM2-FV2 [a,b] | MIROC6 [a] |
| CESM2-WACCM [a,b] | MIROC-ES2L [a] |
| CMCC-CM2-HR4 [a] | MPI-ESM-1-2-HAM |
| CMCC-CM2-SR5 [a] | MPI-ESM1-2-HR |
| CNRM-CM6-1 [a,b] | MPI-ESM1-2-LR |
| CNRM-CM6-1-HR | MRI-ESM2-0 [a,b] |
| CNRM-ESM2-1 [a] | NESM3 |
| E3SM-1-0 | NorCPM1 [a,b] |
| E3SM-1-1 | NorESM2-LM [a] |
| FGOALS-f3-L [a,b] | NorESM2-MM [a] |
| GFDL-CM4 | SAM0-UNICON [a] |
| GFDL-ESM4 | TaiESM1 [a] |
| GISS-E2-1-G [a,b] | UKESM1-0-LL [a] |
| GISS-E2-1-G-CC | |
| GISS-E2-1-H | |

*Note.* The symbol *a* indicates models capable of simulating extreme El Niño events, and the symbol *b* indicates such models that possess an AMIP6 equivalent ensemble presented in Table 1.

models are computed to avoid giving more weight to models with large ensembles (up to 22 members for AMIP6.IPSL-CM6A-LR).

We followed the same methodology as in Beniche et al. (2024) to define ENSO phases using the NOAA Oceanic Niño Index (ONI; Trenberth (2019)), defined as the mean SST anomalies over the Niño3.4 (N3.4) region (5°N–5°S, 170°W–120°W) computed from ERSSTv5, over the boreal winter season. In observations and AMIP6, moderate El Niño events over the 1979–2014 period are categorized by ONI values ranging from +0.5°C to +2°C, La Niña by ONI values lower than −0.5°C and extreme El Niño by ONI values exceeding +2°C (note that for these events, an alternative yet equivalent selection method is used in CMIP6, see Figure 6). Moderate El Niño events are further divided into Central Pacific (CP) and Eastern Pacific (EP) events following the Cold Tongue (CT)/Warm Pool (WP) classification method of Ren and Jin (2011). The results in this paper are robust when using different EP/CP events classification methods. Throughout the paper "moderate El Niño events" refer to CP events (they are all moderate) and moderate EP events. We will show that those two classes (CP and moderate EP events) produce very similar tropical Pacific SST and rainfall distributions (moderate EP events just tend to have larger eastern Pacific SST anomalies than CP events) and very similar teleconnection patterns, justifying their grouping as "moderate events."

We also analyze historical simulations (1850–2014) from 42 CMIP6 models (see Table 2). For model selection, we exclusively consider the first variant, namely "r1i1p1-f1","-f2" or "-f3", depending on availability (we only consider one member per CMIP6 model, even if multiple members are available). To select models able to produce extreme El Niño events, we follow the same procedure as in Cai et al. (2014): we select models exhibiting a DJF Niño3 rainfall anomaly skewness exceeding 1 (the observed 1979–2014 Niño3 rainfall anomaly skewness is 3.7) and producing at least one extreme El Niño event defined by both a Niño3.4 DJF SST anomaly exceeding 0.5 standard deviation (STD) and DJF Niño3 rainfall anomaly greater than 5 mm/day. This method ensures that we only select events associated with a massive reorganization of the eastern Pacific tropical deep convection, a characteristic observed during extreme El Niño events (Cai et al., 2014; Lengaigne & Vecchi, 2009). The extreme El Niño event detection and model selection will be illustrated by Figures 6 and 7 at the beginning of Section 4.

We used the following method to define anomalous DJF climate (e.g., cold or wet) over North America in AMIP6. For each model, we derive average time series of DJF temperature or rainfall anomalies in selected regions (see Figures 2c and 2d). The standard deviation (STD) is computed in each model over 1979–2014 and across ensemble members to ensure statistical robustness. An anomalous event in a given model is identified when the value exceeds the ±0.5 STD threshold (e.g., below −0.5 STD for a dry event). For each ENSO category, the percentage of a given event is computed for each model (across years and ensemble members), and then averaged across models. This ensures that each model's contribution receives equal weight in the MMM analysis. Note that for a normal distribution, an almost equal probability of about 1/3 for each event (e.g., cold, normal, warm) would be expected.

We test whether composites are different from zero at the 97.5% confidence level using a bootstrap resampling (10,000 resampling for models, 1,000 for observations). The lower or upper 2.5% of the distribution allows to determine whether the composite mean is significantly above or below zero.

Finally, we use a Signal-to-Noise ratio (SNR) computation to investigate the causes of the enhanced extreme El Niño reproducibility in AMIP6. The SNR is computed following the Kumar and Hoerling (1995) procedure, where the signal is defined as the forced response to ENSO and the noise as all other signals (e.g., attributable to internal atmospheric variability, or SST-forced signals by other climate modes). This method further allows to

separate the noise into a SST-dependent part (i.e., attributable to the year-to-year SST differences within a given ENSO class) and a (dominant) atmospheric internal variability part. More specifically, this is done as follows. Assume there are M different realizations (years) of a given type of ENSO event (e.g., La Niña) and N ensemble members, internal variability is defined as:

$$\sigma_I^2 = \frac{1}{M*N}\sum_{i=1}^{N}\sum_{\alpha=1}^{M}\left(A_{i\alpha} - \overline{A_\alpha}\right)^2 \quad (1)$$

with $\overline{A_\alpha}$ being the ensemble mean for a specific year. External variability (i.e., atmospheric variability due to changes in SST forcing) is defined as:

$$\sigma_E^2 = \frac{1}{M}\sum_{\alpha=1}^{M}\left(\overline{A_\alpha} - \overline{A}\right)^2 \quad (2)$$

with $\overline{A}$ being the ensemble-mean composite for the considered ENSO event type. Total noise is defined as the square root $\sqrt{\sigma_I^2 + \sigma_E^2}$. Finally, SNR is defined as the ratio $\frac{\text{signal}}{\text{total noise}}$, where the signal is $\overline{A}$ - the multi-model ensemble-mean (MMEM) anomaly amplitude - in the variable's units.

## 3. Extreme El Niño Teleconnection Pattern in AMIP6

In this section, we examine the ability of ensemble simulations from 23 AMIP6 models to reproduce extreme El Niño teleconnection patterns, in order to generalize the results of Beniche et al. (2024) obtained from the CNRM-CM6.1 atmospheric component to the AMIP6 database. We describe the extreme El Niño teleconnection pattern in Section 3.1 and evaluate its reproducibility in Section 3.2.

### 3.1. Extreme El Niño TNH Teleconnection Pattern Across 23 AMIP6 Models

Figures 1a–1h displays AMIP6 multi-model ensemble mean (MMEM) composites of tropical Pacific anomalies and North-American teleconnections for La Niña and moderate CP El Niño events. The tropical Pacific rainfall (PR) anomalies associated with La Niña and moderate CP events have almost the same pattern with opposite signs (Figures 1a and 1e), with either dry or wet anomalies west of the dateline. The resulting teleconnection response also has an opposite sign (negative PNA) and similar magnitude over the North Pacific and North America (Figures 1b and 1f). In other words, the North American rainfall and surface temperature (TS) teleconnection patterns are very similar during La Niña and moderate CP El Niño events. It is noteworthy that the results presented on Figure 1 are robust when the composites are normalized by the mean N3.4 SST anomaly forcing amplitude.

Figure 1 allows comparing the moderate CP El Niño events (panels e–h) with moderate EP El Niño events (panels i–l). Note that usual EP composites retain extreme events, while our moderate EP El Niño composite excludes these events. Only extreme EP events are characterized by SST anomalies that are maximum in the eastern Pacific (panel m), while other EP events simply have larger-amplitude eastern Pacific SST anomalies than CP events (panel f vs. panel e). We did verify that these features are robust when using other CP/EP events classifications (not shown). Despite their stronger eastward extension than during moderate CP El Niño events (Figure 1e vs. Figure 1i), SST anomalies during moderate EP El Niño events are not sufficient to cross the deep atmospheric convective threshold in the eastern Pacific (Beniche et al., 2024; Srinivas et al., 2024). Consequently, the moderate CP and moderate EP equatorial Pacific rainfall anomalies are similar (the moderate EP SST anomaly composite does not peak in the eastern equatorial Pacific, unlike the usual EP composite, due to the exclusion of extreme El Niño events). This comparable zonal distribution of the tropospheric latent heat release gives rise to similar PNA-positive teleconnection patterns over North America (Figures 1f and 1j). The rainfall and surface temperature patterns are also almost similar during moderate CP and moderate EP events (Figures 1g, 1h, 1k and 1l), with wet anomalies confined offshore of the western coast of the USA around 140°W.

During extreme El Niño events, the SST anomalies are sufficiently large to exceed the deep atmospheric convective threshold over a large portion of the eastern Pacific (Figure 1m). Thus, equatorial Pacific rainfall

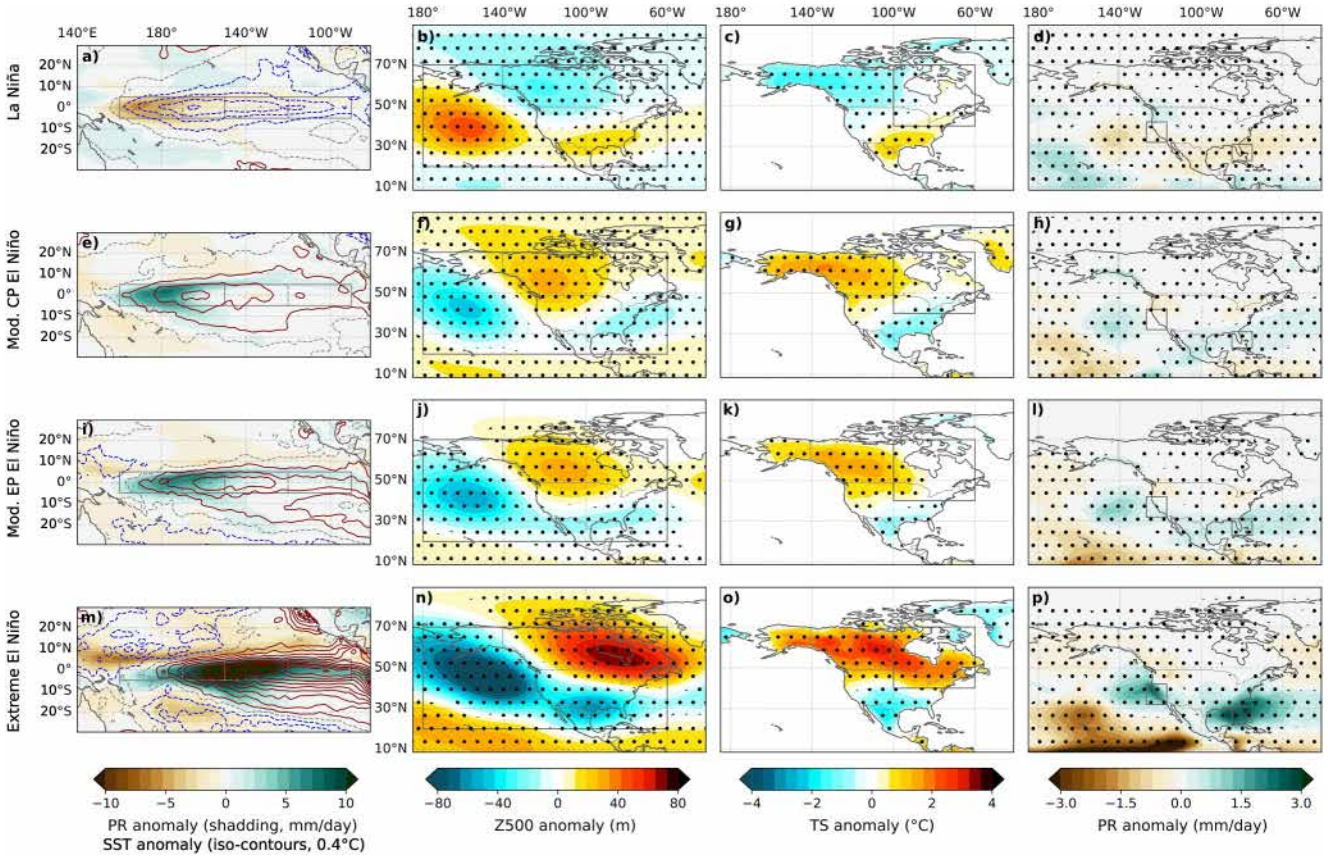


**Figure 1.** 1979–2014 AMIP6 multi-model ensemble-mean (MMEM) winter (DJF) composites for (a–d) La Niña (e–h) moderate CP El Niño (f–i) moderate EP El Niño and (m–p) extreme El Niño, for (left) tropical Pacific rainfall (PR) anomaly (shading, mm/day) and HadISST anomaly (contours, 0.4°C, dotted contours for negative values), and North Pacific-North American (middle left) 500 hPa geopotential height (Z500) anomaly (m), (middle right) land surface temperature (TS) anomaly (°C) and (right) rainfall (PR) anomaly (mm/day). The composites are not normalized. Dots indicate regions where anomalies are significantly different of zero at the 97.5% confidence level based on a bootstrap test with 10,000 resamples. See Table 1 for the list of the 23 AMIP6 ensemble simulations, and the number of members available for each.

anomalies extend further east than during La Niña and moderate CP and EP El Niño events (Figures 1a– 1e and 1f). This substantial and eastward-shifted tropospheric latent heat release during extreme El Niño events results in a similarly substantial and eastward-shifted Z500 response over North America (compare Figures 1n–1p with panels above). Consequently, the poleward advection of warm anomalies extends further east over North America, influencing northeastern America (Figure 1o). The change in rainfall teleconnection pattern is a bit less clear, and for instance mainly features a strengthening of the wet signal over Florida. Yet, there is a clear eastward shift of the wet anomalies that are offshore during moderate El Niño events, but stand clearly over the western U. S. coastline, including California, during extreme El Niño events. In summary, the MMEM from 23 AMIP6 models is very similar to the extreme El Niño specific teleconnection pattern identified in the AMIP6-CNRM. CM6-1 by Beniche et al. (2024).

Figure 2 shows the extreme minus moderate El Niño teleconnection pattern, allowing to examine their differences (we remind that, throughout this article, "moderate El Niño" refers to both moderate CP and moderate EP El Niño events). In this instance, anomalies have been normalized by the amplitude of the mean N3.4 SST anomaly forcing prior to compositing, with the objective of focusing on differences in patterns rather than differences in amplitude. However, the results remain robust if this normalization is not performed. The eastward shift of the equatorial Pacific tropospheric heat source, the resulting eastward shift of the North American Z500 PNA response toward the TNH pattern of Wallace and Gutzler (1981); Mo and Livezey (1986); Livezey and Mo (1987), the occurrence of extra wet anomalies over California and Florida, and extra warm anomalies over the Northeast U.S. are all statistically significant in the AMIP6 MMEM (and in observations, see Supplementary Figure S1 in Supporting Information S1).

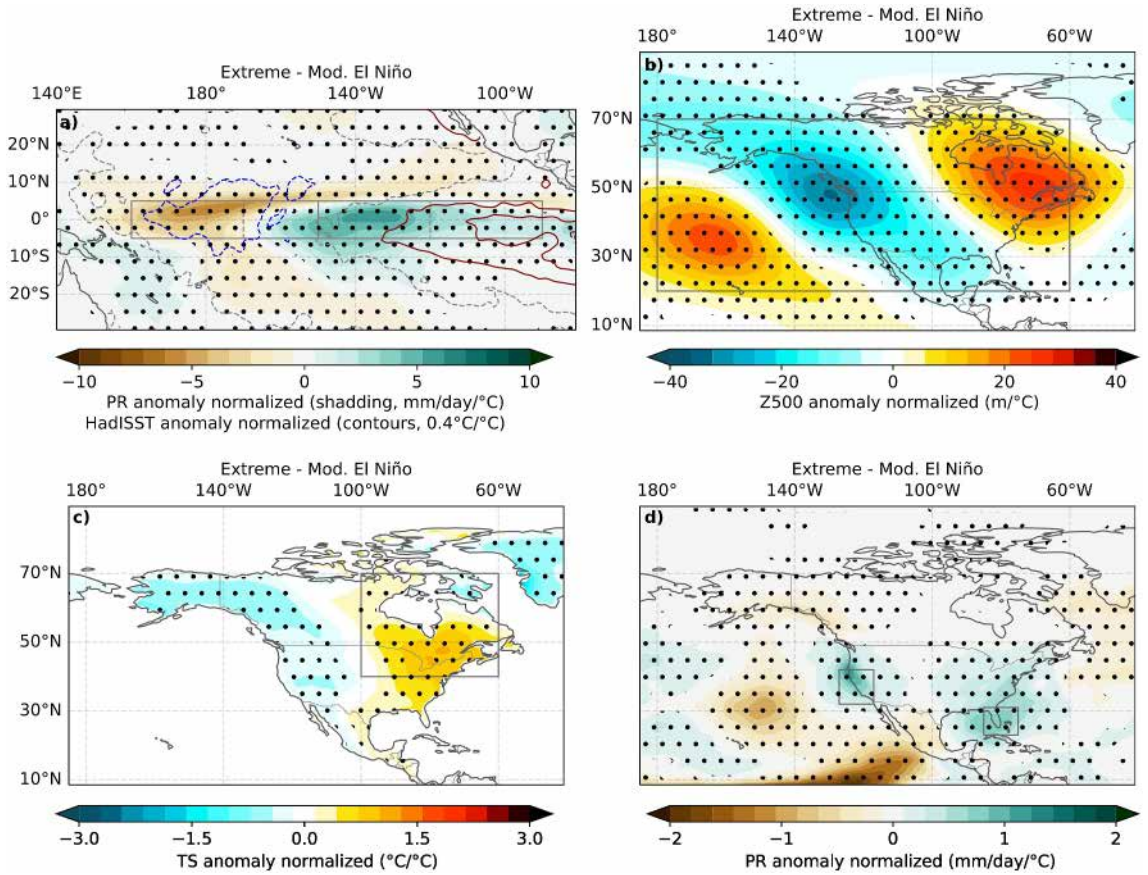


**Figure 2.** Extreme minus moderate El Niño MMEM winter (DJF) composites, for (a) tropical rainfall (shaded, mm/day/°C) and SST anomalies (contours, red for positive and blue for negative, 0.4°C/°C), and North Pacific-North American (b) 500 hPa geopotential height (m/°C), (c) land surface temperature (°C/°C), and (d) rainfall anomalies (mm/day/°C). Each composite is obtained after normalizing by the N3.4 SST anomaly, in order to emphasize the pattern rather than the amplitude differences (see Methods for details). Dots indicate areas where anomalies are significantly different from zero at the 97.5% confidence level based on a bootstrap test with 10,000 resamples.

As previously demonstrated, the eastward shift and distinctive teleconnections over North America during extreme El Niño events discussed in (Beniche et al., 2024) are robust in the AMIP6 MMEM. We now investigate whether these features are similarly robust across individual AMIP6 model ensemble means. Figure 3 displays the normalized extreme minus moderate El Niño ensemble mean composites (i.e., Figure 2b) but for each of the 23 AMIP6 models. All models exhibit a pattern correlation to the MMEM AMIP6 difference greater than 0.5. More than half (12) of the models exhibit a pattern correlation above 0.8. This indicates a high degree of agreement with the AMIP6 MMEM. The ability of each model to replicate the eastward-shifted TNH-like pattern during extreme El Niño events can be evaluated by comparing the tripole structure in the extreme minus moderate El Niño teleconnection composite in this model to that of the AMIP6 MMM (Figure 3 bottom right panel). Some models fail to reproduce the PNA-like teleconnection pattern (see Supplementary Figure S6 in Supporting Information S1), though they still capture the TNH-like pattern during extreme events. One model fails to produce the characteristic tripole pattern, showing instead a more intense PNA structure during extreme El Niño events. Therefore, we conclude that the distinctive TNH-like teleconnection pattern of extreme El Niño relative to the PNA-like teleconnection pattern of moderate El Niño events is a robust feature in 22 out of 23 AMIP6 ensemble simulations.

### 3.2. Extreme El Niño Teleconnections Reproductibility in AMIP6

Beniche et al. (2024) demonstrate that the extreme El Niño teleconnection pattern to North America is reproducible across events and ensemble members in their CNRM-CM6.1 atmospheric component 16-member ensemble. They assumed the high reproducibility of the Z500 pattern and associated PR and TS anomalies

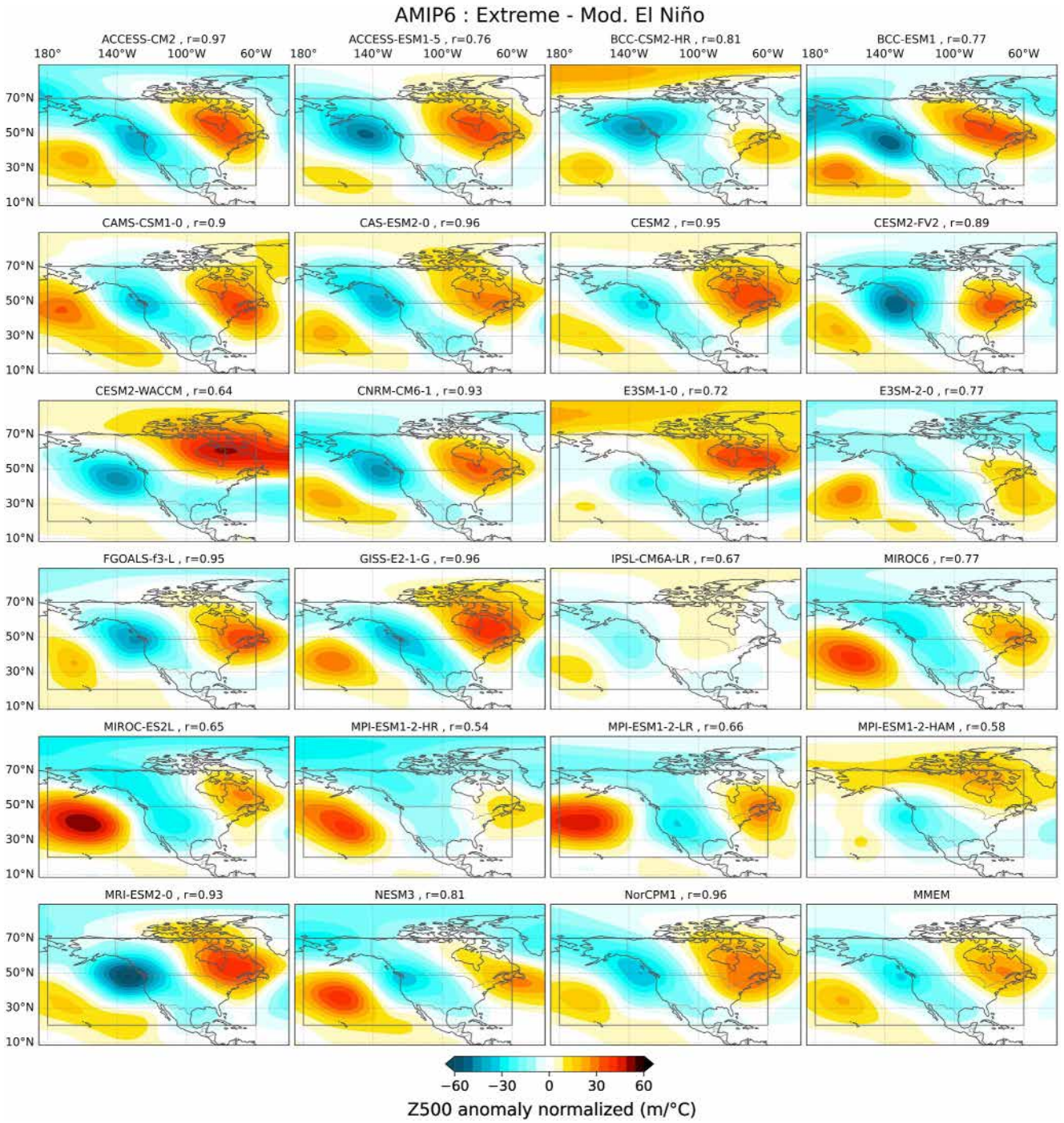


**Figure 3.** Extreme El Niño minus moderate El Niño ensemble-mean winter (DJF) 500 hPa anomalies (m/°C) composites for AMIP6 individual models, and for the multi-model ensemble mean (MMEM) in the lower right panel. Each composite is obtained after normalizing by the N3.4 SST anomaly (see Methods for details). The name of the model, and the pattern correlation to the AMIP6 MMEM difference (computed over the 180–60°W, 20–70°N black frame) are indicated above each panel. Details of the ensemble-mean composites for each model, separately analyzed for moderate and extreme El Niño events, are presented in Supplementary Figure S6 in Supporting Information S1.

were due to a higher Signal-to-Noise ratio during extreme El Niño events. In this subsection, we examine the robustness of the extreme El Niño teleconnection pattern reproducibility in the larger AMIP6 ensemble and investigate the reason behind it.

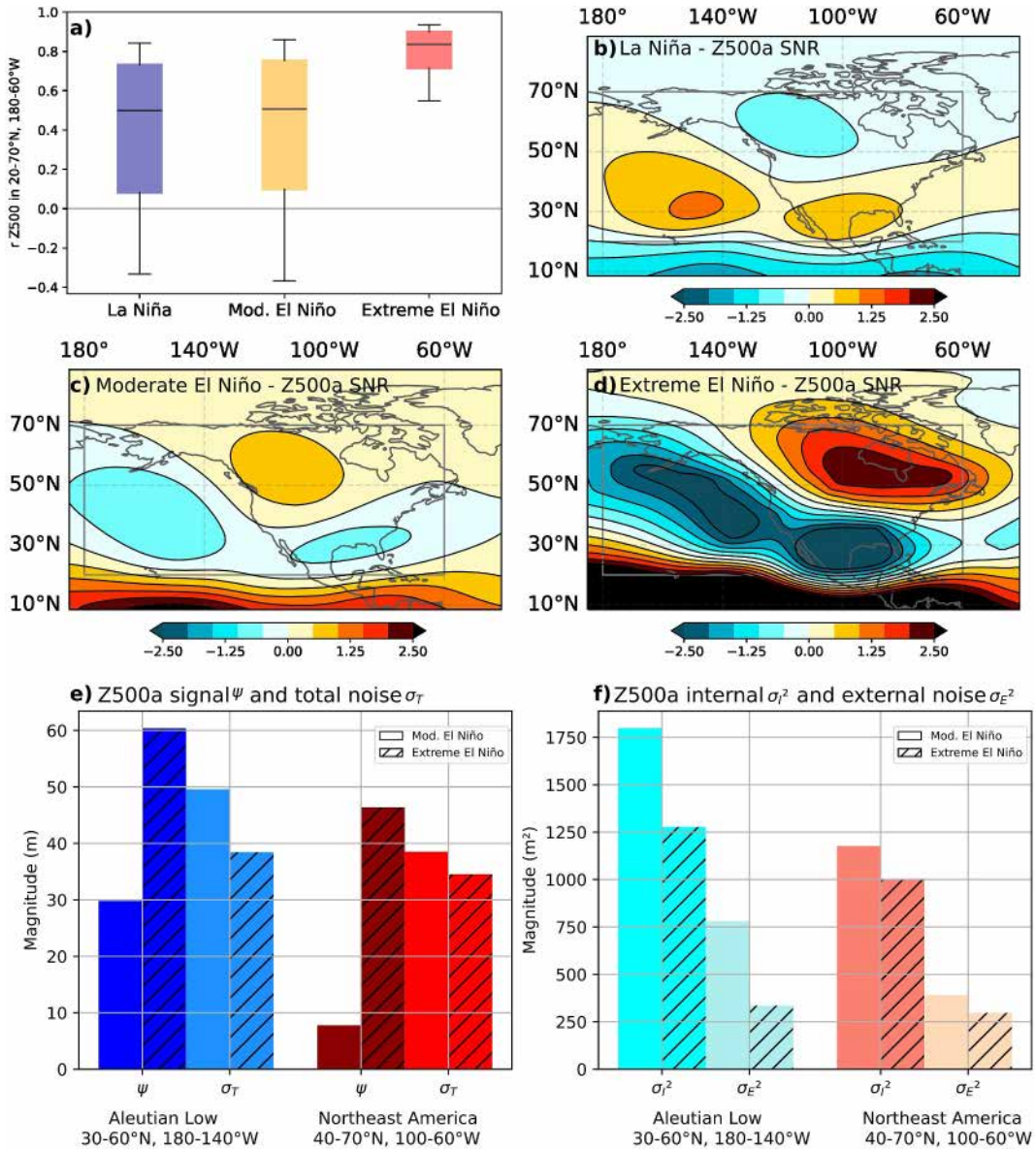


**Figure 4.** (a) Reproducibility of the DJF 500-hPa geopotential height anomalies during La Niña (blue), moderate El Niño (yellow) and extreme (red) El Niño events. The whiskers indicate the 10th and 90th percentiles and boxes the 25th, 50th (horizontal line) and 75th percentiles of the pattern correlation between the Z500 anomalies from each member, model, and event to the MMEM composite of the corresponding ENSO phase. The pattern correlation is computed within the box on panels (b)–(d): 20–70°N, 180–60°W. 500-hPa geopotential height anomalies MMEM Signal-to-Noise ratio (SNR) for (b) La Niña, (c) moderate El Niño and (d) extreme El Niño events. The SNR represents the ratio of the MMEM signal for a given event to the spread associated to both the internal variability, and inter-event SST-driven variability (diversity of SST patterns within a given ENSO type class, see Methods for details). (e) AMIP6 MMEM moderate (plain) and extreme (hatching) El Niño Aleutian Low region (shades of blue [30–60°N, 180–140°W]) and Northeast America (shades of red [40–70°N, 100–60°W]) DJF 500 hPa geopotential height anomaly signal Ψ and total atmospheric noise $\sigma_T$. (f) Decomposition of total noise $\sigma_T^2$ into internal atmospheric variability $\sigma_I^2$ and inter-event SST-forcing diversity $\sigma_E^2$ contributions.

Figure 4a displays the distributions of the pattern correlation of Z500 anomalies across the North Pacific-North America in each member to the multi-model ensemble for La Niña, moderate El Niño and extreme El Niño MMEM composites, respectively. For La Niña and moderate El Niño, the median pattern correlation is only 0.5, indicating that anomalies in an individual ensemble member are a mixture of the ENSO signal and noise associated with internal atmospheric variability (e.g., Deser et al. (2017)). This explains why pattern correlations range from negative values (might be due to strong internal variability signatures) to values above 0.9 (weak

internal variability signatures). In contrast, for extreme El Niño, the median pattern correlation is approximately 0.85, with 90% of values exceeding 0.6. This implies that the North American Z500 realization in each member of each model during each analyzed extreme El Niño (1982–1983 and 1997–1998) is highly similar to the MMEM composite pattern displayed on Figure 1n. This therefore confirms that the considerably greater reproducibility of extreme El Niño teleconnections in comparison to other ENSO categories (La Niña, moderate El Niño) in the AMIP CNRM-CM6.1 ensemble is a robust finding within the broader AMIP6 database.

Figures 4b–4d illustrates the La Niña, moderate and extreme El Niño MMEM Z500 teleconnection Signal-to-Noise ratios (SNR) as defined in the Method section. In agreement with previous studies (Horel & Wallace, 1981; Kumar & Hoerling, 1995), our analysis points to regions of SNR exceeding 0.5 in the vicinity of the PNA extrema during La Niña and moderate El Niño, indicating that this teleconnection pattern is associated with a satisfying potential for predictability over North America. The SNR values are considerably higher (1–2.5) during extreme El Niño events, which explains the high reproducibility of North American Z500 anomalies during these events. Figure 4e further compares the signal and noise amplitudes around two regions of high SNR during moderate and extreme El Niño events. The stronger signal is the primary factor contributing to the favorable SNR during extreme events: the amplitude of the mean Z500 anomaly signal is more than doubled, while noise only decreases by about 20% from a moderate to an extreme El Niño. Figure 4f further indicates that the noise is mostly dominated by atmospheric internal variability, with a smaller contribution of SST pattern diversity within a given ENSO category.

Figures 5a–5c illustrates the reproducibility of wet anomalies over California and Florida, and warm anomalies over Northeast America during extreme El Niño events. It should be noted that the averaging regions have been modified from Beniche et al. (2024) to focus on the specific extreme El Niño signature observed in AMIP6 in Figure 1. However, our results remain robust to both area selections. In addition, a new region around Florida has been introduced (see frame on Figure 2d). There is no discernible shift in the probability distribution for the Californian rainfall and Northeast American surface temperature during La Niña or moderate El Niño events. In both cases, the median remains close to zero, and positive and negative anomalies are equally probable. The situation is markedly different for extreme El Niño events, with a pronounced shift in the distribution and 69%/77% chances of warm/wet anomalies (defined as exceeding the 0.5 std threshold, see Methods). The situation is somewhat different for Florida, where a minor shift toward dry anomalies occurs during La Niña and toward wet anomalies during moderate El Niño events. The shift to wet anomalies is, however, much more pronounced and systematic during extreme El Niño events, with a 97% probability of wet anomalies. These reproducible signals during extreme El Niño events are due to high SNR values (greater than 1, Figures 5d and 5e). The enhanced reproducibility observed during extreme El Niño events and over Florida compared to California is a consequence of the stronger signals (see SNR decomposition in Supplementary Figure S2 in Supporting Information S1).

This section presents evidence that extreme El Niño events are associated with a distinct teleconnection pattern over Northern America. This pattern is shifted eastward relative to the typical PNA pattern, resembles the Tropical-Northern Hemisphere (TNH) pattern, and is associated with higher probabilities of rainfall over California, Florida, and warm anomalies over Northeast America. This pattern is highly reproducible across the 270 realizations of the 1982/1983 and 1997/1998 extreme El Niño realizations (i.e., 135 ensemble members) from 23 AMIP6 models, a result largely attributable to larger signals than those observed during moderate El Niño or La Niña events.

## 4. Do CMIP6 Models Reproduce the Specific Extreme El Niño Teleconnections?

### 4.1. Selecting Models That Produce Extreme El Niño Events

This section examines the influence of the SST equatorial cold bias in CMIP6 models on the reproduction of extreme El Niño teleconnection pattern relatively to AMIP6. CMIP6 models are selected based on their ability to reproduce the large observed eastern Pacific rainfall anomalies during extreme El Niño events, which is essential to generating their specific teleconnection (Beniche et al., 2024). We show that these models are generally characterized by a weaker cold tongue bias than other CMIP6 models. We will then compare the extreme El Niño teleconnection pattern and North American impacts in those models with those in AMIP6 (we will discuss taking the AMIP6 MMM as a reference in the final section).

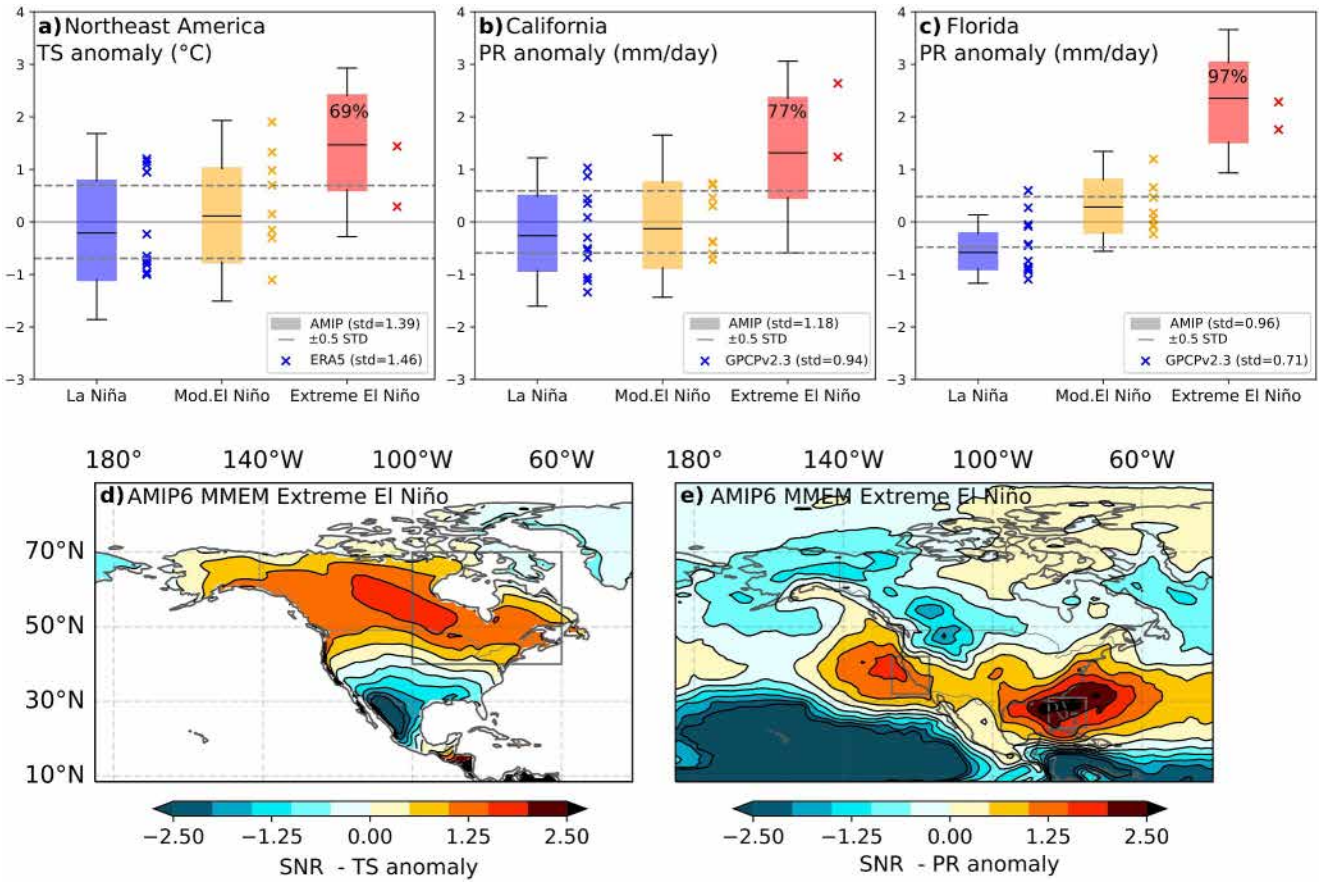


**Figure 5.** (a) Distribution of mean Northeast American (40–70°N, 100–60°W) DJF land surface temperature anomalies (°C) in the entire AMIP6 multi model ensemble for La Niña (blue), moderate El Niño (orange) and extreme El Niño (red) events. The whiskers indicate the 10th and 90th percentiles and boxes the 25th, 50th (horizontal line) and 75th percentiles. The crosses indicate observed ERA5 surface temperature anomalies for each event in a given category. The AMIP6 MMEM and ERA5 anomalies standard deviation are indicated in the inlay. Dotted lines mark ± 0.5 STD (from the MMEM value). (b) Same as (a) but for California (32–42°N, 133–123°W) rainfall anomalies. (c) Same as (a) but for Florida (23–30°N, 85–75°W) rainfall anomalies. (d) MMEM composite signal-to-noise ratio (SNR) for extreme El Niño land surface temperature anomalies. The Northeast American box used in (a) is plotted. (e) Same as (d) but for rainfall anomalies SNR, with the California and Florida boxes plotted.

Here, we briefly illustrate our method for detecting extreme El Niño events in CMIP6 (see Section 2). In order to trigger the specific TNH pattern, extreme El Niño events must be associated with large eastern Pacific rainfall anomalies (Beniche et al., 2024). We therefore use the criteria proposed by Cai et al. (2014), which defines extreme El Niño based on their ability to generate such anomalies. Figure 6 illustrates this extreme El Niño detection method for observations and one CMIP6 model example (here, CMIP6. CNRM-CM6.1). In observations and AMIP6, the two extreme El Niño events during the 1979–2014 period (1982/1983 and 1997/1998, both with Niño3.4 SSTa above 2 STD) meet such criteria, with Niño3 rainfall anomalies exceeding 5 mm/day. For the CMIP6. CNRM-CM6.1 164-year historical simulation (1850–2014), two extreme El Niño events are identified (Niño3.4 SSTa greater than 0.5 STD and Niño3 rainfall anomalies greater than 5 mm/day), one of them being displayed on Figures 6c and 6d which shows a subset of the simulation that matches the observational records on panels a,b. Due to the limitation of rainfall and SST records before the satellite era (before the 1980s), and the modulation of the tropical SST variability by tropical decadal variability (Latif et al., 1997; Power et al., 2021), there is a considerable uncertainty in the number of observed extreme El Niño events using this criterion. There are for instance two extreme El Niño events over our 1979–2014 reference period, but a third one in 2015/16, giving a range of 5–7 events per century for the post-1979 satellite area.

A total of 42 CMIP6 models, as listed in Table 2, are analyzed. Figure 7 displays their DJF Niño3-average rainfall anomalies skewness (SKW) computed over 164 years (1850–2014). The MMM SKW is underestimated (2.2) in comparison to observations (3.7) and AMIP6 (3.3) over recent decades (1979–2014) and the majority of models

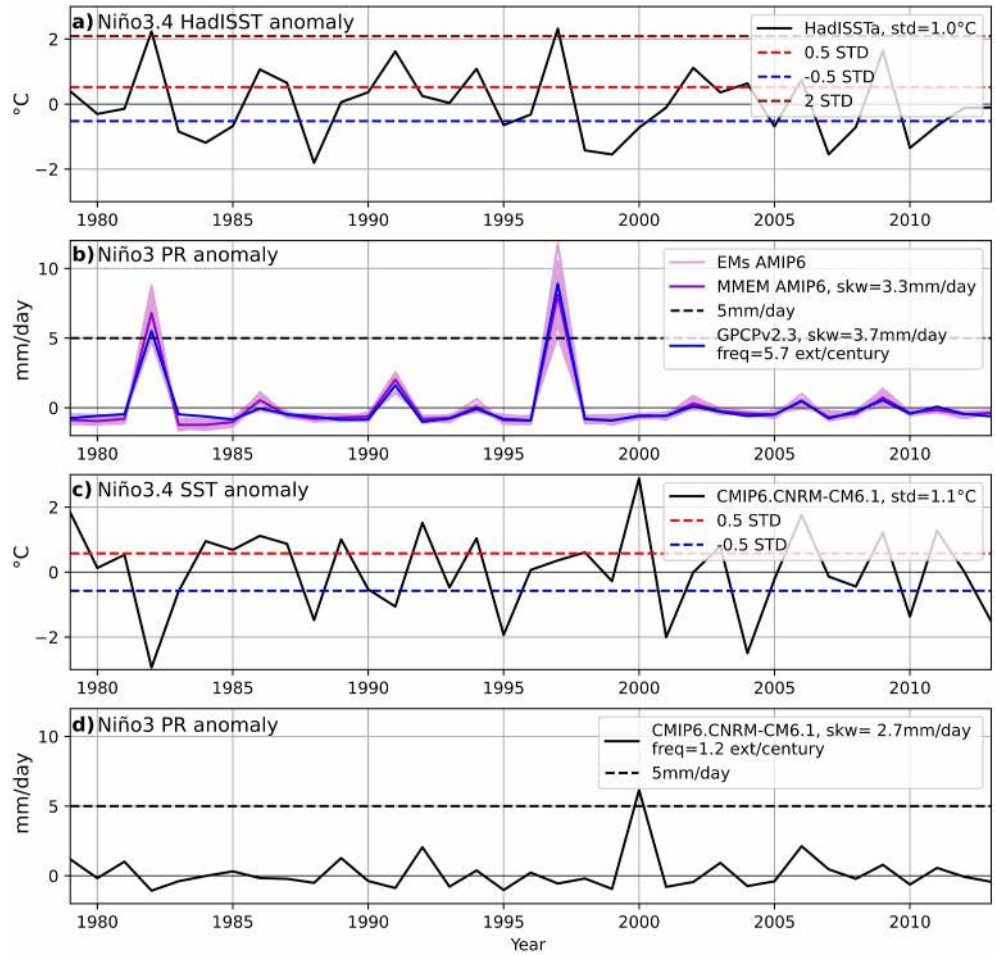


**Figure 6.** (a) 1979–2014 time series of DJF mean N3.4 HadISST SST anomalies. Dashed lines indicates the −0.5, +0.5 and +2 STD thresholds. (b) 1979–2014 time series of DJF mean N3 rainfall anomalies from individual AMIP6 ensemble-means (pink), the AMIP6 MMEM (purple) and GPCPv2.3 observations (blue). The dashed line indicates the +5 mm/day threshold. (c) 1979–2014 time series of DJF mean N3.4 SST anomalies from the CMIP6. CNRM-CM6.1 historical simulation. Dashed lines indicate the −0.5, +0.5 STD threshold. (d) Same as (c) but for the mean Niño3 PR anomaly. Dashed line indicates the +5 mm/day threshold. This figure illustrates our method for detecting extreme El Niño events in CMIP6, defined as El Niño events (Niño3.4 SSTA > 0.5 STD) with Niño3 average rainfall anomalies above 5 mm/day.

exhibit such underestimation (33 out of 42 models under 3). Six models exhibit a Niño3 rainfall anomaly SKW below 1, thus failing to meet the SKW criterion (red bars). These models consistently fail to produce extreme rainfall in association with El Niño events (see the extreme El Niño frequency above each bar). In addition, 10 models with a Niño3 rainfall anomaly skewness above 1 are rejected, as they are unable to produce El Niño events with Niño3 rainfall anomalies exceeding 5 mm/day (orange bars). Consequently, we select 26 out of 42 CMIP6 models that verify the rainfall-based extreme El Niño detection criteria of Cai et al. (2014), with a mean extreme El Niño frequency of 4 events per century, against 5 to 6 over the satellite era in observations and the AMIP6 ensemble (Figure 7a). Among the 26 selected models, corresponding AMIP6 simulations are available for 11 of them, which allows for a comparison of extreme El Niño teleconnection patterns between AMIP6 and CMIP6 in those models.

Bayr et al. (2024) have related the ability of CMIP6 models to produce large eastern Pacific rainfall anomalies to the amplitude of their cold tongue bias. Figure 8 compares the equatorial Relative Sea Surface Temperature (RSST) bias in the selected and rejected (i.e., those that fail to produce extreme rainfall in the eastern Pacific) CMIP6 models. The RSST proxy is employed here because it is a reliable indicator of atmospheric stability (Izumo et al., 2020; Xie et al., 2010) and it effectively removes tropical average biases, which do not influence the convective threshold (Johnson & Xie, 2010). The selected models exhibit a weaker MMM cold bias than the

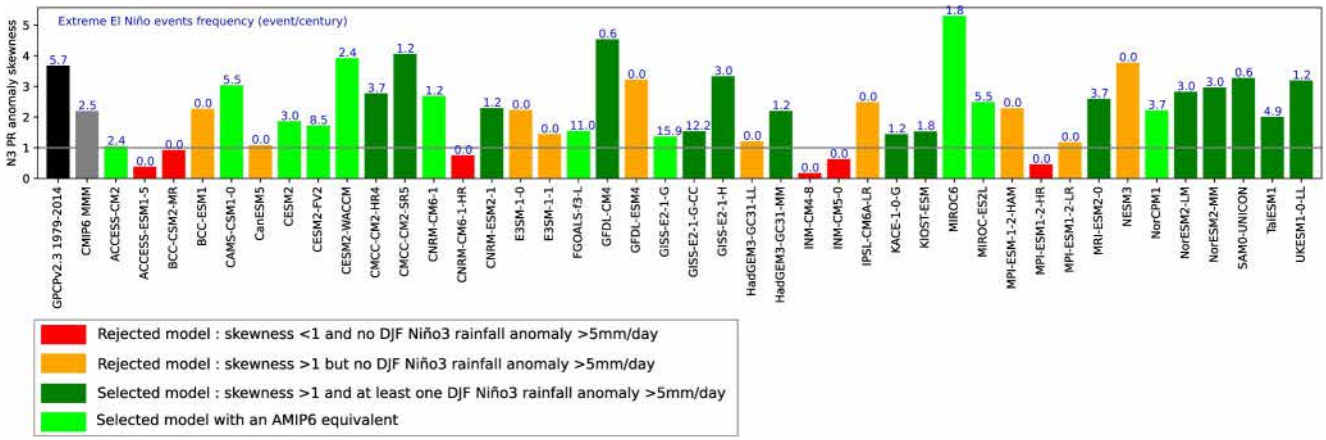


**Figure 7.** Bar plot of the Niño3 rainfall anomaly skewness (SKW) for GPCPv2.3 (1979–2014 period) and the 42 considered CMIP6 models (1850–2014 period). The extreme El Niño occurrence frequency (event/century, with extreme El Niño events defined as N3.4 SSTA exceeding 0.5 STD and N3 rainfall anomalies exceeding 5 mm/day) is indicated above each bar. Red bars indicate rejected models because their N3 rainfall skewness is below 1. Orange bars indicate rejected models because they do not produce any extreme El Niño event. Dark green bars indicate selected models for which no corresponding AMIP6 simulation is available. Light green bars indicate selected models for which an AMIP6 simulation is available. Within 42 examined CMIP6 models, 16 are rejected, and 26 selected (11 of which have an AMIP6 equivalent).

rejected ones over most of the central and western Pacific. Furthermore, the central Pacific bias distributions do not overlap. Consistent with the reduced cold bias, the selected models display a reduced western to central equatorial Pacific dry bias, with non-overlapping distributions (Figure 8b). While the rejected models produce positive SST anomalies in Niño3, their cold RSST bias results in absolute RSST that does not exceed zero, thus preventing deep atmospheric convection and rainfall above 5 mm/day in Niño3 (Figure 8c). Finally, Figure 7d illustrates the number of extreme eastern Pacific rainfall events per century as a function of the RSST bias. A positive RSST bias is not a sufficient condition to produce extreme eastern Pacific rainfall, as seven models with positive RSST bias do not produce them. However, it is a necessary condition to produce more than two events per century (the observed value over the satellite period being 7–8). In summary, our findings corroborate the relationship between the cold tongue bias and the ability to generate large wet eastern Pacific events, as previously proposed by Bayr et al. (2024).

### 4.2. CMIP6 Models Reproduce the Teleconnection Shift Between Moderate and Extreme El Niño Events

Figure 9 provides the MMM of the moderate and extreme El Niño teleconnection patterns for the 26 selected CMIP6 models. In general, the CMIP6 teleconnection patterns are relatively similar to those in AMIP6 (pattern correlation with the AMIP6 MMEM above 0.9 for Z500, 0.7 for surface temperature and 0.8 for rainfall, Figure 9). The CMIP6 MMM reproduces the eastward shift of the AMIP6 extreme El Niño teleconnection pattern relative to that of moderate events (shown in Figure 1). In particular, the Z500 anomaly for moderate El Niño events displays a typical PNA pattern, while extreme El Niño events exhibit a TNH-like pattern, with positive Z500 anomalies shifted eastward to over the Hudson Bay (Figures 9a and 9d). The warm anomalies similarly shift from Alaska and western Canada to central and eastern Canada. The rainfall response also strengthens and shifts eastward, as in AMIP6, the only difference being that California also experiences mild rainfall anomalies during moderate El Niño events in the CMIP6 MMM. In summary, the MMM of CMIP6 models that are capable of simulating extreme El Niño events also captures the distinct TNH-like teleconnection pattern of extreme El Niño events, shifted eastward relative to that of moderate events. The MMM CMIP6 La Niña teleconnection pattern is similar to that in AMIP6, also corresponding to a negative PNA pattern (not shown).

Next, we investigate how individual CMIP6 models reproduce the AMIP6 MMEM, eastward-shifted teleconnection pattern. Figure 9g displays a Taylor diagram (Taylor, 2001) evaluating each selected CMIP6 model Z500 extreme El Niño composite against that of the AMIP6 MMEM. 18 out of 26 models lie within the 30 m RMS error contour, and have pattern correlations with the AMIP6 MMEM pattern above 0.8 and a pattern amplitude within ±30% of the observed value, that is, have similar extreme El Niño teleconnections to our AMIP6 MMEM reference. On the other hand, 8 CMIP6 models have significantly degraded extreme El Niño

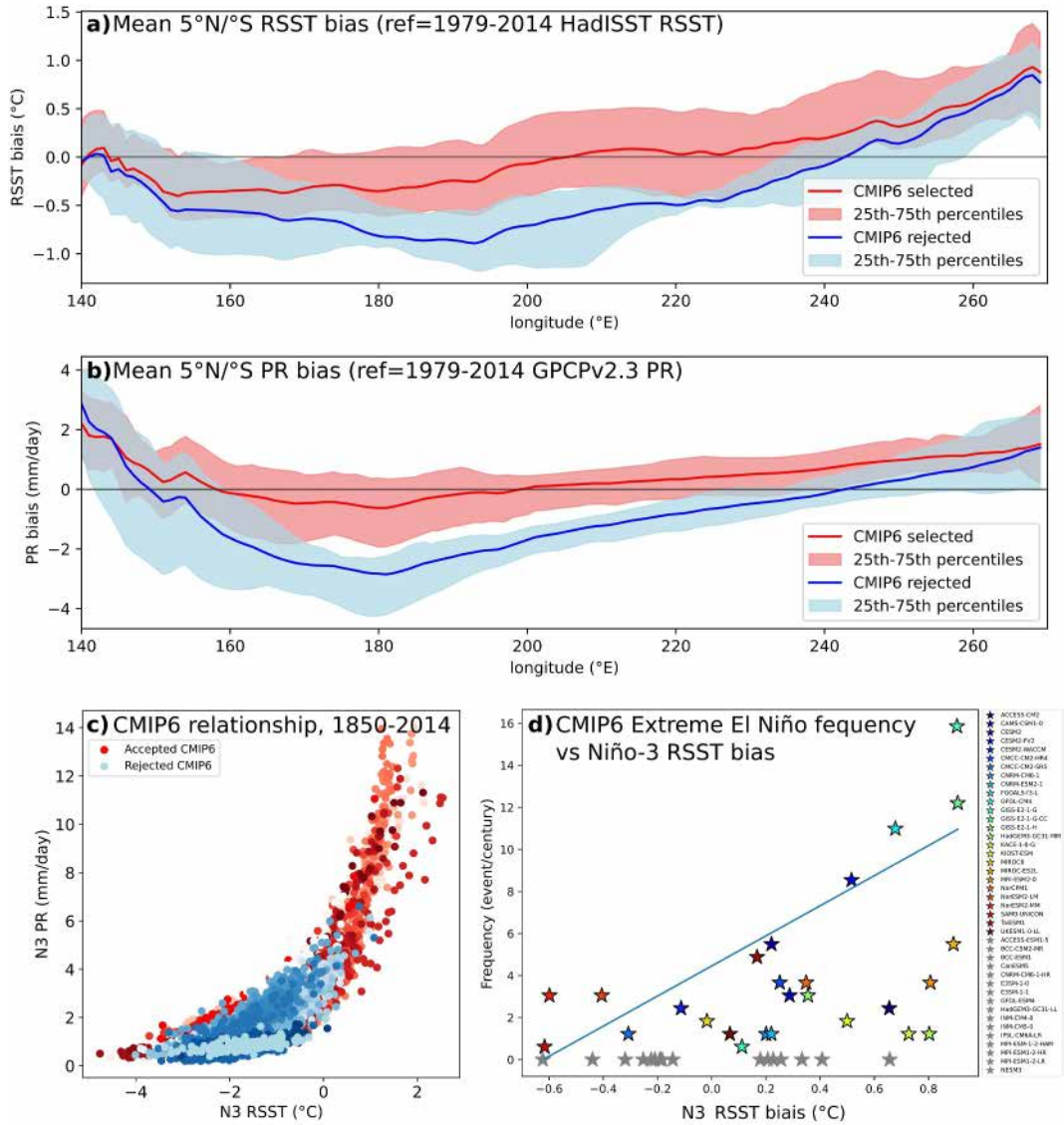


**Figure 8.** (a) 5°N–5°S average RSST bias (°C) for the 26 selected (red) and 16 rejected (blue) CMIP6 models. The line indicates the MMM, shading the 25th–75th percentile based on a bootstrap test with 10,000 resampling. The bias is calculated with respect to 1870–2014 average HadISST data. (b) Same as (a), but for precipitation (mm/day) and 1979–2014 average GPCPv2.3 data. (c) Scatterplot of Niño3 average rainfall (mm/day) against the Niño3 RSST bias (RSST correspond to Niño3 SST minus the 20°N–20°S average SST for each model). Selected models are in red, and rejected in blue, with different shades of red/blue indicating different models in each group. (d) Extreme El Niño occurrence frequency (event/century) as a function of the Niño3 RSST bias (°C) for the 42 CMIP6 models (rejected models are in gray).

teleconnection patterns relative to the AMIP6 MMEM, with pattern correlations as low as 0.3 and over or underestimated magnitudes by a factor of two. In summary, 18 of the 26 models that reproduce extreme El Niño events have a very comparable extreme El Niño teleconnection pattern to that from the AMIP6 MMEM.

Above, we have compared the AMIP6 MMEM to all the CMIP6 models that produce extreme eastern Pacific rainfall anomalies (26 models). The specificity of the extreme El Niño teleconnection pattern remains robust when only considering the subset of selected CMIP6 models for which an AMIP6 simulation is available (11 models, see Figure S3 in Supporting Information S1). Within this subset, we can investigate how CMIP models' SST biases, particularly the equatorial Pacific "cold tongue bias", affect extreme El Niño teleconnections. Figure 10a presents a Taylor diagram of the MMM Z500 extreme El Niño teleconnection pattern over the North Pacific-North American box for these 11 AMIP6 models and their CMIP6 counterparts (the reference being the

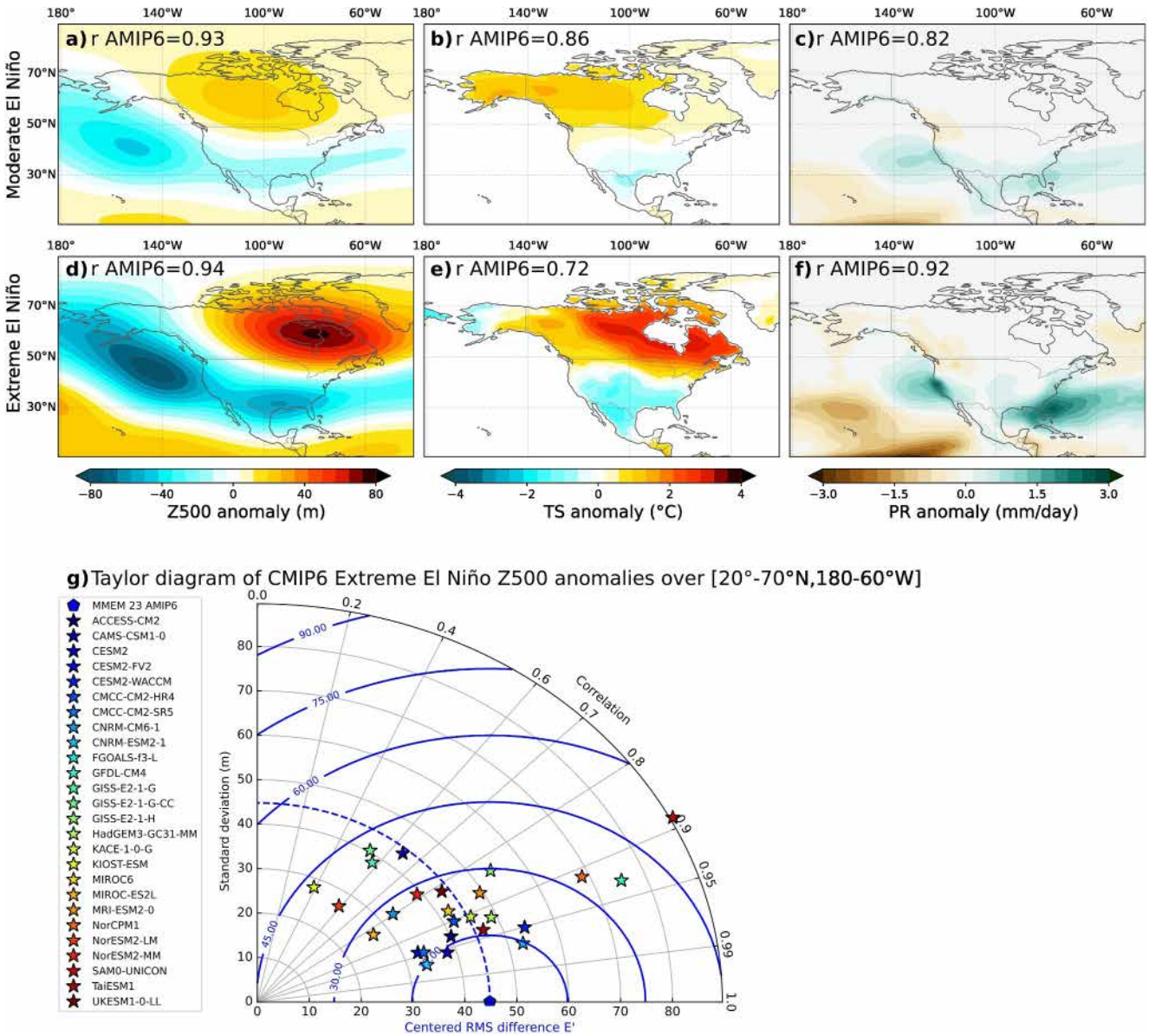


**Figure 9.** Multi model Mean 500-hPa geopotential height anomaly composites from all 26 CMIP6 models (able to perform extreme El Niño events), for moderate El Niño (a) DJF GPH 500-hPa anomaly (m), (b) land surface temperature anomaly (°C) and rainfall anomaly (mm/day), and extreme El Niño (e), (f), (g). The term r AMIP6 indicates the pattern correlation over the entire plotted area with the composite and its corresponding AMIP6 MMEM from Figure 1. (g) Taylor Diagram for the North Pacific-North American Z500 anomalies extreme El Niño teleconnection pattern for the 26 individual selected CMIP6 models. The reference data set (black pentagon on the *x*-axis) is the Z500 extreme El Niño composite from the AMIP6 MMEM.

AMIP6 MMEM). The MMM for these common models (yellow and purple stars) indicates a slight extreme El Niño teleconnection pattern degradation (0.99–0.96 pattern correlation) and amplitude decay (45–36 m) from AMIP6 to CMIP6. Next, individual models are considered. Green arrows link each CMIP6 score to that of its corresponding AMIP6 model, allowing to gauge the impact of SST biases in each model. For all models, arrows point to a region with a lower pattern correlation with the reference pattern. More specifically, all AMIP6 models have a pattern correlation above 0.85 while 4 of the corresponding CMIP6 models drop to a range between 0.55 and 0.85. All models except 3 also display a teleconnection with a weaker amplitude than that of the reference AMIP6 MMEM, with amplitude underestimations of up to 40% in CMIP6. Overall, the MMM AMIP6 extreme El Niño teleconnection pattern is quite well reproduced by the CMIP6 ensemble mean. The CMIP6 extreme El Niño

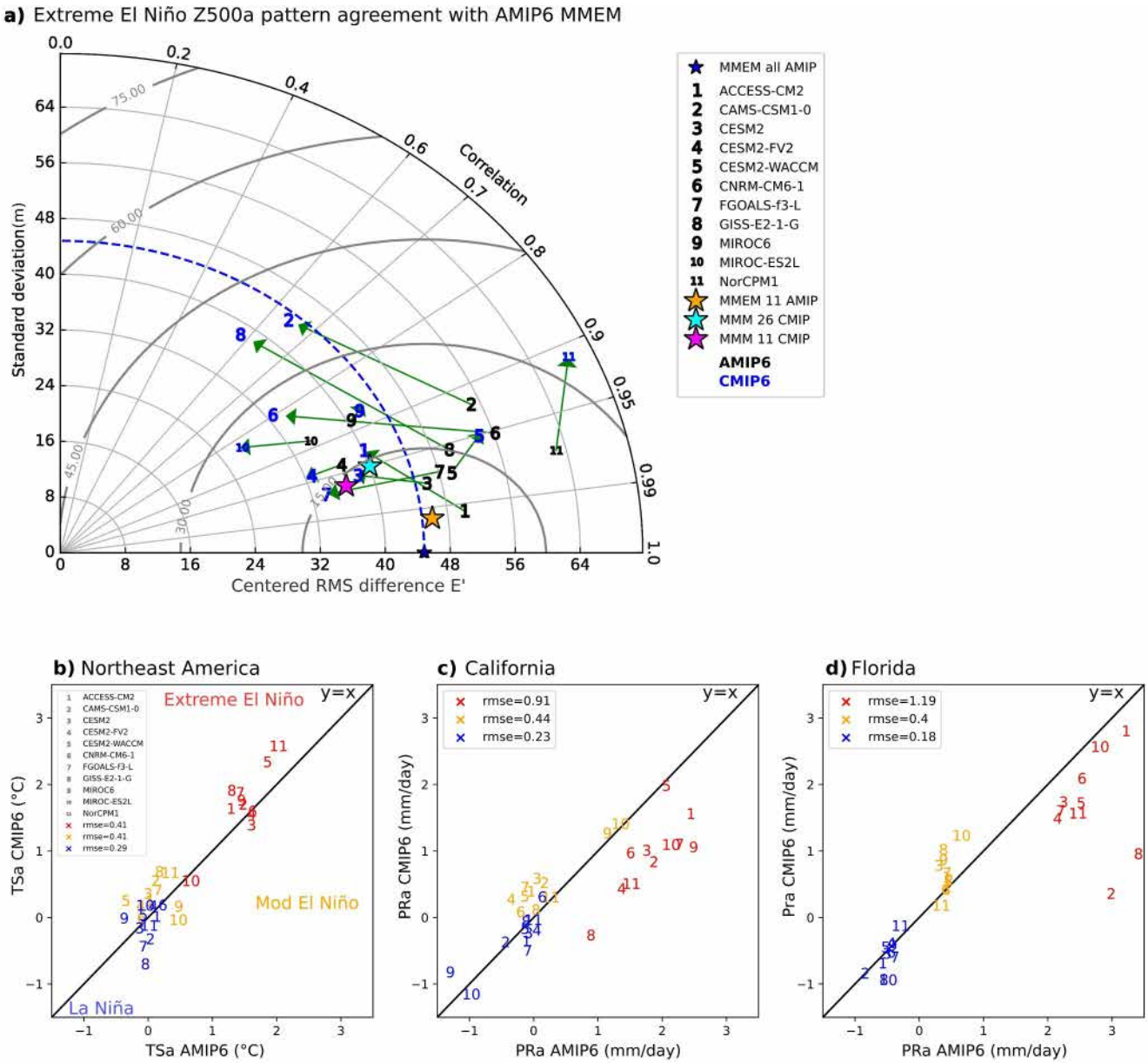


**Figure 10.** (a) Taylor diagram of North Pacific-North American extreme El Niño 500 hPa geopotential height anomaly for the 11 common AMIP6 (black numbers) and CMIP6 (blue numbers) ensemble-mean composite. Direction of the green arrows indicates how the pattern and amplitude change from the AMIP6 to the CMIP6 model version, where the radius represents the standard deviation (STD) and the angle, the pattern correlation value. (b) Model-means of land surface temperature (°C) anomaly composites averaged over the Northeast America box (40–70°N, 100–60°W) from the 11 AMIP6 and CMIP6 commons models, for La Niña (blue), moderate El Niño (orange) and extreme El Niño (red). Anomalies are not normalized. (c) Same as (b) but for rainfall (mm/day) anomalies averaged over California. (d) Same as (b) but for rainfall (mm/day) anomalies averaged over Florida.

teleconnection pattern remains reasonable in 18 individual CMIP6 models, but is degraded relative to its AMIP6 counterpart in some.

Next, this section compares the surface temperature and rainfall impacts of ENSO between the CMIP6 and AMIP6, for the 11 selected CMIP6 models with AMIP6 counterparts, and for the three regions already discussed in Figure 5 (Northeast America, California, Florida). CMIP6 models display a comparable surface temperature response over Northeast America to their AMIP6 counterpart across ENSO phases. All the models except for one display a pronounced warming over North America during extreme El Niño, in both AMIP6 and CMIP6. Over California and Florida, CMIP6 and AMIP6 models tend to agree during La Niña and moderate El Niño events. In

contrast, the California and Florida CMIP6 rainfall response to extreme El Niño events is notably reduced relative to its AMIP6 counterpart (57%/40% reduction for the MMM over California/Florida, with a much more severe reduction in some models and even the wrong sign in one model).

In this section, we have demonstrated that 16 out of the 42 CMIP6 models considered are unable to simulate extreme El Niño events (El Niño events with >5 mm/day rainfall anomalies in the eastern Pacific). These models are associated with colder equatorial cold tongue bias. The MMM of the 26 CMIP6 models capable of simulating extreme El Niño events reproduces the distinct eastward shift from a Pacific-North American (PNA) toward a Tropical-Northern Hemisphere (TNH) teleconnection pattern during these events, consistent with AMIP6. However, the teleconnection pattern is generally degraded in CMIP6 models relative to their AMIP6 counterparts, significantly degraded in 8 of the 26 selected CMIP6 models, and CMIP6 models tend to underestimate the extreme El Niño wet anomalies over California and Florida.

## 5. Summary and Discussion

### 5.1. Summary

Beniche et al. (2024) found that both La Niña and moderate El Niño exhibit a Pacific-North American (PNA) boreal winter teleconnection pattern, and that only extreme El Niño events such as the 1982–1983, 1997–1998 and 2015–2016 events lead to a significant eastward shift of that teleconnection pattern toward a Tropical-Northern Hemisphere (TNH) pattern, associated with strong and reproducible surface temperature and rainfall anomalies over North America. Their results were however obtained from a 16-member ensemble with a single AMIP6 model (namely, the CNRM-CM6.1 atmospheric component), and hence are subject to model error and noise from internal variability. Here, we first investigate the robustness of their results using a broader AMIP6 data set, comprising 23 different models and a total 135 members covering 1979–2014. This provides 270 realizations for the two extreme El Niño events of 1982–1983 and 1997–1998. Our analysis confirms that the PNA teleconnection during moderate ENSO events only shifts to the specific TNH teleconnection pattern during extreme El Niño events. It also confirms that the associated climate impacts are very reproducible, with 69% chances of warm (> 0.5 STD) anomalies over Northeastern America, and 77%/97% of wet anomalies over California/Florida across the entire AMIP6 database. We attribute those more systematic impacts than those during moderate El Niño or La Niña events to a much more reproducible Z500 teleconnection pattern during extreme El Niño events. Our large database permitted a Signal-to-Noise ratio analysis that was not possible from the Beniche et al. (2024) limited ensemble, confirming that this increased reproducibility stems from a large signal relative to the atmospheric internal variability.

Our second objective was to examine if the SST biases that develop in CMIP6 models impact their ability to produce a distinct teleconnection pattern during extreme El Niño events. Among the 42 examined CMIP6 models, 16 fail to produce extreme El Niño events, defined based on their ability to produce large (> 5 mm/day) eastern Pacific rainfall anomalies during a warm event, as in Cai et al. (2014); Lengaigne and Vecchi (2009). These models tend to have a strong equatorial Pacific cold SST bias, as already noted by Bayr et al. (2024), which inhibits tropical deep atmospheric convection development in the eastern Pacific. A near-zero or positive RSST bias is necessary (but not sufficient) for CMIP6 models to be able to develop extreme eastern Pacific wet anomalies. The MMM teleconnection patterns from the 26 CMIP6 models that produce such extreme eastern Pacific wet anomalies successfully reproduce PNA-like teleconnections for moderate El Niño (and La Niña) and TNH-like teleconnections exclusively for extreme El Niño events, in agreement with AMIP6. While reasonable in 18 of those 26 models, the CMIP6 teleconnection pattern is however degraded relatively to its AMIP6 counterpart, with a lower pattern correlation to and generally weaker amplitude than the AMIP6 MMEM reference pattern. CMIP6 models underestimate wet anomalies over California and Florida during extreme El Niño events, while they generally reproduce the AMIP6 moderate El Niño and La Niña weaker teleconnection signals.

### 5.2. Discussion and Perspectives

Previous studies have discussed the sources of diversity in the ENSO teleconnection patterns, with some studies identifying a different teleconnection pattern between CP and EP events (Ashok et al., 2007; Garfinkel et al., 2012), and others concluding that a convective anomaly is necessary in the eastern-central Pacific (Chiodi & Harrison, 2015; Johnson & Kosaka, 2016). Consistent with other work (Hoell et al., 2016; Jong et al., 2016) our study shows that, as far as Northern America is concerned, only extreme El Niño events (i.e., EP events that have

both large SST and convective anomalies in the eastern Pacific) really induce a major change in the teleconnection pattern. The moderate CP and EP events composites of Figure 1 take advantage of the large AMIP6 database (675 moderate CP events and 405 moderate EP events realizations). Although this large database reveals significant differences between the moderate CP and EP events normalized patterns, such as an enhanced warming over eastern United States of America and slightly stronger wet anomalies over Florida (Supplementary Figure S4 in Supporting Information S1), these differences are very weak compared to those between extreme and moderate El Niño events. The observed composites for moderate CP and EP events are more different than those in AMIP6 (Supplementary Figure S5 in Supporting Information S1), although less significant and noisier. The observed teleconnection patterns for moderate EP events closely resemble the canonical PNA pattern and associated anomalies, while those for moderate CP El Niño events are somewhat different. Previous studies have however warned that such observed patterns are highly subject to modification from internal atmospheric variability (Deser et al., 2017). In addition, our record only contains 3 moderate EP events, implying that the observed (and AMIP6 MMEM) patterns may also contain signatures from SST anomalies that are not related to ENSO. We suggest, in line with previous studies (e.g., Brands (2017)), that the observed differences between moderate CP and moderate EP events are mainly associated with those ENSO-independent SST anomalies and internal atmospheric variability. In summary, we think that the strong inter-model agreement and large number of realization in AMIP6 strongly supports the view that the main source of ENSO teleconnection diversity over Northern America is associated with extreme El Niño events.

The recent 2015/2016 extreme El Niño event was associated with prolonged drought over California, with significant societal impacts (Seager et al., 2015). The seasonal forecasts, on the other hand, projected wet anomalies (S. Lee et al., 2018; Paek et al., 2017), possibly due to overestimated eastern Pacific warm and convective anomalies (Jong et al., 2018; Paek et al., 2017). The study of Beniche et al. (2024) also included the 2015–2016 event (and concluded to 74% chances of wet anomalies), while our study only covers the 1982–1983 and 1997–1998 events (with a similar probability of wet conditions of 77%). One possibility for this mismatch may be due to the weaker prolonged eastern Pacific warming after the 2015–2016 El Niño peak (S. Lee et al., 2018), or to internal variability as the observed anomalies do fall within the range of possible forecast outcomes (Jong et al., 2018; Kumar & Chen, 2016). Nevertheless, our AMIP6 ensemble still indicates a 10% chance of dry anomalies over California during the 1982–1983 and 1997–1998 extreme El Niño events (Figure 5b). Our results are thus also consistent with the observed dry anomalies over California in 2015–2016, if we consider a probabilistic rather than deterministic approach.

In this study, we considered the Multi-Model Ensemble Mean AMIP6 ENSO teleconnection pattern as a reference to gauge the quality of those in CMIP6. This is motivated by the fact that the strong aliasing by internal atmospheric variability strongly limits the knowledge of ENSO teleconnection patterns (Deser et al., 2017; Garfinkel et al., 2012), but of course limited by potential common biases to all AMIP6 models. One could further argue that the inclusion of air-sea coupling in coupled models (e.g., see Brands (2022); Guilyardi et al. (2009)) is an added level of realism that may improve extratropical teleconnections (Mori et al., 2024), and more generally ENSO teleconnections. Our findings however indicate a very similar shift from the PNA to the TNH pattern in presence of extreme El Niño events in AMIP6 and most CMIP6 models, suggesting that coupling processes may not be a major influence on extratropical teleconnection patterns.

Climate projections from CMIP models suggest an enhanced eastern and central Pacific warming in response to climate change, or "El Niño-like" warming (e.g., Power et al. (2021)). Notwithstanding recent observations of subdued warming in the eastern and central Equatorial Pacific (e.g., Heede and Fedorov (2023a); Power et al. (2021)), this "El Niño-like" warming reduces the barrier to deep-atmospheric convection in the eastern Pacific, with a strong influence on ENSO projections. CMIP6 models indeed project both more frequent extreme eastern Pacific rainfall response to ENSO, and more frequent extreme eastern Pacific SST anomalies (Cai et al., 2021; Heede & Fedorov, 2023c; Shin et al., 2022). A promising avenue for future research is to investigate the consequence of our results for future projections. Our results indeed indicate that 18 CMIP6 models reproduce extreme El Niño events and their specific, eastward-shifted teleconnection pattern. The reinforced and eastward shifted ENSO teleconnection pattern seen in some studies (e.g., Drouard and Cassou (2019); McGregor et al. (2022); Zhou et al. (2014); Müller and Roeckner (2008); Johnson et al. (2022); Michel et al. (2020)) could thus be partly interpreted as an increased frequency of the TNH-like pattern associated with extreme El Niño events, rather than a change in the teleconnection pathway. In addition, it will also be valuable to assess the impact

of the biases in the CMIP6 ENSO teleconnection patterns on future projections, especially over California where CMIP6 already tends to underestimate extreme El Niño rainfall anomalies in the current climate.

## Conflict of Interest

The authors declare no conflicts of interest relevant to this study.

## Data Availability Statement

The ECMWF Reanalysis v5 (ERA5) monthly averaged is available from Copernicus at https://cds.climate.copernicus.eu/datasets/reanalysis-era5-pressure-levels-monthly-means?tab=overview. The Global Precipitation Climatology Project (GPCP) v2.3 data set is available from https://www.ncei.noaa.gov/data/global-precipitation-climatology-project-gpcp-monthly/. The HadISST version 1.1 monthly reanalysis data are available from https://www.metoffice.gov.uk/hadobs/hadisst/data/download.html. The AMIP6 and CMIP6 from the Coupled Model Intercomparison Project Phase 6 archives are freely available from https://esgf-node.ipsl.upmc.fr/search/cmip6-ipsl/.

**Acknowledgments**
Margot Beniche's PhD grant was funded under the French Agence Nationale pour la Recherche (ANR) ARISE project (ANR-18-CE01-0012)and partially supported through the grant EUR TESS N°ANR-18-EURE-0018 in the framework of the Programme des Investissements d'Avenir. We thank the 2 anonymous reviewers for their comments, which helped to improve the manuscript, and Christophe Cassou, for insightful discussions that inspired the AMIP6 analysis.

## References

Adler, R., Sapiano, M., Huffman, G., Wang, J.-J., Gu, G., Bolvin, D., et al. (2018). The global precipitation climatology project (GPCP) monthly analysis (new version 2.3) and a review of 2017 global precipitation. *Atmosphere*, *9*(4), 138. https://doi.org/10.3390/atmos9040138

Ashok, K., Behera, S. K., Rao, S. A., Weng, H., & Yamagata, T. (2007). El niño modoki and its possible teleconnection. *Journal of Geophysical Research*, *112*(C11). https://doi.org/10.1029/2006jc003798

Barnston, A. G., & Livezey, R. E. (1987). Classification, seasonality and persistence of low-frequency atmospheric circulation patterns. *Monthly Weather Review*, *115*(6), 1083–1126. https://doi.org/10.1175/1520-0493(1987)115⟨1083:csapol⟩2.0.co;2

Bayr, T., Lübbecke, J. F., Vialard, J., & Latif, M. (2024). Equatorial pacific cold tongue bias degrades simulation of enso asymmetry due to underestimation of strong eastern pacific el niños. *Journal of Climate*, *37*(23), 6167–6182. https://doi.org/10.1175/jcli-d-24-0071.1

Bellenger, H., Guilyardi, E., Leloup, J., Lengaigne, M., & Vialard, J. (2013). Enso representation in climate models: From cmip3 to cmip5. *Climate Dynamics*, *42*(7–8), 1999–2018. https://doi.org/10.1007/s00382-013-1783-z

Beniche, M., Vialard, J., Lengaigne, M., Voldoire, A., Srinivas, G., & Hall, N. M. J. (2024). A distinct and reproducible teleconnection pattern over north America during extreme el niño events. *Scientific Reports*, *14*(1), 2457. https://doi.org/10.1038/s41598-024-52580-9

Brands, S. (2017). Which enso teleconnections are robust to internal atmospheric variability? *Geophysical Research Letters*, *44*(3), 1483–1493. https://doi.org/10.1002/2016gl071529

Brands, S. (2022). A circulation-based performance atlas of the cmip5 and 6 models for regional climate studies in the northern hemisphere mid-to-high latitudes. *Geoscientific Model Development*, *15*(4), 1375–1411. https://doi.org/10.5194/gmd-15-1375-2022

Cai, W., Borlace, S., Lengaigne, M., van Rensch, P., Collins, M., Vecchi, G., et al. (2014). Increasing frequency of extreme el niño events due to greenhouse warming. *Nature Climate Change*, *4*(2), 111–116. https://doi.org/10.1038/nclimate2100

Cai, W., Santoso, A., Collins, M., Dewitte, B., Karamperidou, C., Kug, J.-S., et al. (2021). Changing el niño–southern oscillation in a warming climate. *Nature Reviews Earth & Environment*, *2*(9), 628–644. https://doi.org/10.1038/s43017-021-00199-z

Capotondi, A., Wittenberg, A. T., Newman, M., Lorenzo, E. D., Yu, J.-Y., Braconnot, P., et al. (2015). Understanding ENSO diversity. *Bulletin of the American Meteorological Society*, *96*(6), 921–938. https://doi.org/10.1175/bams-d-13-00117.1

Chiodi, A. M., & Harrison, D. E. (2013). El niño impacts on seasonal u.s. atmospheric circulation, temperature, and precipitation anomalies: The OLR-event perspective. *Journal of Climate*, *26*(3), 822–837. https://doi.org/10.1175/jcli-d-12-00097.1

Chiodi, A. M., & Harrison, D. E. (2015). Global seasonal precipitation anomalies robustly associated with el niño and la niña events—An OLR perspective. *Journal of Climate*, *28*(15), 6133–6159. https://doi.org/10.1175/jcli-d-14-00387.1

Deser, C., Simpson, I. R., McKinnon, K. A., & Phillips, A. S. (2017). The northern hemisphere extratropical atmospheric circulation response to enso: How well do we know it and how do we evaluate models accordingly? *Journal of Climate*, *30*(13), 5059–5082. https://doi.org/10.1175/jcli-d-16-0844.1

Deser, C., Simpson, I. R., Phillips, A. S., & McKinnon, K. A. (2018). How well do we know enso's climate impacts over north America, and how do we evaluate models accordingly? *Journal of Climate*, *31*(13), 4991–5014. https://doi.org/10.1175/jcli-d-17-0783.1

Drouard, M., & Cassou, C. (2019). A modeling- and process-oriented study to investigate the projected change of enso-forced wintertime teleconnectivity in a warmer world. *Journal of Climate*, *32*(23), 8047–8068. https://doi.org/10.1175/jcli-d-18-0803.1

Eyring, V., Bony, S., Meehl, G. A., Senior, C. A., Stevens, B., Stouffer, R. J., & Taylor, K. E. (2016). Overview of the coupled model intercomparison project phase 6 (cmip6) experimental design and organization. *Geoscientific Model Development*, *9*(5), 1937–1958. https://doi.org/10.5194/gmd-9-1937-2016

Feng, J., Chen, W., & Li, Y. (2016). Asymmetry of the winter extra-tropical teleconnections in the northern hemisphere associated with two types of enso. *Climate Dynamics*, *48*(7–8), 2135–2151. https://doi.org/10.1007/s00382-016-3196-2

Garfinkel, C. I., Hurwitz, M. M., Waugh, D. W., & Butler, A. H. (2012). Are the teleconnections of central pacific and eastern pacific el niño distinct in boreal wintertime? *Climate Dynamics*, *41*(7–8), 1835–1852. https://doi.org/10.1007/s00382-012-1570-2

Garfinkel, C. I., Weinberger, I., White, I. P., Oman, L. D., Aquila, V., & Lim, Y.-K. (2018). The salience of nonlinearities in the boreal winter response to enso: North pacific and north America. *Climate Dynamics*, *52*(7–8), 4429–4446. https://doi.org/10.1007/s00382-018-4386-x

Guilyardi, E., Wittenberg, A., Fedorov, A., Collins, M., Wang, C., Capotondi, A., et al. (2009). Understanding el niño in ocean–atmosphere general circulation models: Progress and challenges. *Bulletin of the American Meteorological Society*, *90*(3), 325–340. https://doi.org/10.1175/2008bams2387.1

Heede, U. K., & Fedorov, A. V. (2023a). Colder eastern equatorial pacific and stronger walker circulation in the early 21st century: Separating the forced response to global warming from natural variability. *Geophysical Research Letters*, *50*(3). https://doi.org/10.1029/2022gl101020

Heede, U. K., & Fedorov, A. V. (2023b). Towards understanding the robust strengthening of enso and more frequent extreme el niño events in cmip6 global warming simulations. *Climate Dynamics*. https://doi.org/10.1007/s00382-023-06856-x

Heede, U. K., & Fedorov, A. V. (2023c). Towards understanding the robust strengthening of enso and more frequent extreme el niño events in cmip6 global warming simulations. *Climate Dynamics*. https://doi.org/10.1007/s00382-023-06856-x

Hersbach, H., Bell, B., Berrisford, P., Hirahara, S., Horányi, A., Muñoz-Sabater, J., et al. (2020). The ERA5 global reanalysis. *Quarterly Journal of the Royal Meteorological Society*, *146*(730), 1999–2049. https://doi.org/10.1002/qj.3803

Hoell, A., Hoerling, M., Eischeid, J., Wolter, K., Dole, R., Perlwitz, J., et al. (2016). Does el niño intensity matter for California precipitation? *Geophysical Research Letters*, *43*(2), 819–825. https://doi.org/10.1002/2015gl067102

Hoerling, M. P., & Kumar, A. (2002). Atmospheric response patterns associated with tropical forcing. *Journal of Climate*, *15*(16), 2184–2203. https://doi.org/10.1175/1520-0442(2002)015⟨2184:arpawt⟩2.0.co;2

Hoerling, M. P., Kumar, A., & Zhong, M. (1997). El niño, la niña, and the nonlinearity of their teleconnections. *Journal of Climate*, *10*(8), 1769–1786. https://doi.org/10.1175/1520-0442(1997)010⟨1769:enolna⟩2.0.co;2

Horel, J. D., & Wallace, J. M. (1981). Planetary-scale atmospheric phenomena associated with the southern oscillation. *Monthly Weather Review*, *109*(4), 813–829. https://doi.org/10.1175/1520-0493(1981)109⟨0813:psapaw⟩2.0.co;2

Hoskins, B. J., & Karoly, D. J. (1981). The steady linear response of a spherical atmosphere to thermal and orographic forcing. *Journal of the Atmospheric Sciences*, *38*(6), 1179–1196. https://doi.org/10.1175/1520-0469(1981)038⟨1179:tslroa⟩2.0.co;2

Izumo, T., Vialard, J., Lengaigne, M., & Suresh, I. (2020). Relevance of relative sea surface temperature for tropical rainfall interannual variability. *Geophysical Research Letters*, *47*(3). https://doi.org/10.1029/2019gl086182

Johnson, N. C., & Kosaka, Y. (2016). The impact of eastern equatorial pacific convection on the diversity of boreal winter el niño teleconnection patterns. *Climate Dynamics*, *47*(12), 3737–3765. https://doi.org/10.1007/s00382-016-3039-1

Johnson, N. C., Wittenberg, A. T., Rosati, A. J., Delworth, T. L., & Cooke, W. (2022). Future changes in boreal winter enso teleconnections in a large ensemble of high-resolution climate simulations. *Frontiers in Climate*, *4*. https://doi.org/10.3389/fclim.2022.941055

Johnson, N. C., & Xie, S.-P. (2010). Changes in the sea surface temperature threshold for tropical convection. *Nature Geoscience*, *3*(12), 842–845. https://doi.org/10.1038/ngeo1008

Jong, B.-T., Ting, M., & Seager, R. (2016). El niño's impact on California precipitation: Seasonality, regionality, and el niño intensity. *Environmental Research Letters*, *11*(5), 054021. https://doi.org/10.1088/1748-9326/11/5/054021

Jong, B.-T., Ting, M., Seager, R., Henderson, N., & Lee, D. E. (2018). Role of equatorial pacific sst forecast error in the late winter California precipitation forecast for the 2015/16 el niño. *Journal of Climate*, *31*(2), 839–852. https://doi.org/10.1175/jcli-d-17-0145.1

Kug, J.-S., Jin, F.-F., & An, S.-I. (2009). Two types of el niño events: Cold tongue el niño and warm pool el niño. *Journal of Climate*, *22*(6), 1499–1515. https://doi.org/10.1175/2008jcli2624.1

Kumar, A., & Chen, M. (2016). What is the variability in us west coast winter precipitation during strong el niño events? *Climate Dynamics*, *49*(7–8), 2789–2802. https://doi.org/10.1007/s00382-016-3485-9

Kumar, A., & Hoerling, M. P. (1995). Prospects and limitations of seasonal atmospheric GCM predictions. *Bulletin of the American Meteorological Society*, *76*(3), 335–345. https://doi.org/10.1175/1520-0477(1995)076⟨0335:palosa⟩2.0.co;2

Kumar, A., & Hoerling, M. P. (1998). Annual cycle of pacific–north american seasonal predictability associated with different phases of enso. *Journal of Climate*, *11*(12), 3295–3308. https://doi.org/10.1175/1520-0442(1998)011⟨3295:acopna⟩2.0.co;2

Latif, M., Kleeman, R., & Eckert, C. (1997). Greenhouse warming, decadal variability, or el niño? An attempt to understand the anomalous 1990s. *Journal of Climate*, *10*(9), 2221–2239. https://doi.org/10.1175/1520-0442(1997)010⟨2221:gwdvoe⟩2.0.co;2

Lee, J., Julien, P. Y., & Lee, S. (2023). Teleconnection of enso extreme events and precipitation variability over the United States. *Journal of Hydrology*, *619*, 129206. https://doi.org/10.1016/j.jhydrol.2023.129206

Lee, S., Lopez, H., Chung, E., DiNezio, P., Yeh, S., & Wittenberg, A. T. (2018). On the fragile relationship between el niño and California rainfall. *Geophysical Research Letters*, *45*(2), 907–915. https://doi.org/10.1002/2017gl076197

Lengaigne, M., & Vecchi, G. A. (2009). Contrasting the termination of moderate and extreme el niño events in coupled general circulation models. *Climate Dynamics*, *35*(2–3), 299–313. https://doi.org/10.1007/s00382-009-0562-3

L'Heureux, M. L., Levine, A. F. Z., Newman, M., Ganter, C., Luo, J., Tippett, M. K., & Stockdale, T. N. (2020). Enso prediction. *Wiley*, 227–246. https://doi.org/10.1002/9781119548164.ch10

Li, R. K. K., Woollings, T., O'Reilly, C., & Scaife, A. A. (2020). Effect of the north pacific tropospheric waveguide on the fidelity of model el niño teleconnections. *Journal of Climate*, *33*(12), 5223–5237. https://doi.org/10.1175/jcli-d-19-0156.1

Liu, F., Vialard, J., Fedorov, A. V., Éthé, C., Person, R., Zhang, W., & Lengaigne, M. (2024). Why do oceanic nonlinearities contribute only weakly to extreme el niño events? *Geophysical Research Letters*, *51*(11). https://doi.org/10.1029/2024gl108813

Livezey, R. E., & Mo, K. C. (1987). Tropical-extratropical teleconnections during the northern hemisphere winter. part II: Relationships between monthly mean northern hemisphere circulation patterns and proxies for tropical convection. *Monthly Weather Review*, *115*(12), 3115–3132. https://doi.org/10.1175/1520-0493(1987)115⟨3115:tetdtn⟩2.0.co;2

McGregor, S., Cassou, C., Kosaka, Y., & Phillips, A. S. (2022). Projected enso teleconnection changes in cmip6. *Geophysical Research Letters*, *49*(11). https://doi.org/10.1029/2021gl097511

McPhaden, M. J., Zebiak, S. E., & Glantz, M. H. (2006). ENSO as an integrating concept in earth science. *Science*, *314*(5806), 1740–1745. https://doi.org/10.1126/science.1132588

Michel, C., Li, C., Simpson, I. R., Bethke, I., King, M. P., & Sobolowski, S. (2020). The change in the enso teleconnection under a low global warming scenario and the uncertainty due to internal variability. *Journal of Climate*, *33*(11), 4871–4889. https://doi.org/10.1175/jcli-d-19-0730.1

Mo, K. C. (2010). Interdecadal modulation of the impact of enso on precipitation and temperature over the United States. *Journal of Climate*, *23*(13), 3639–3656. https://doi.org/10.1175/2010jcli3553.1

Mo, K. C., & Livezey, R. E. (1986). Tropical-extratropical geopotential height teleconnections during the northern hemisphere winter. *Monthly Weather Review*, *114*(12), 2488–2515. https://doi.org/10.1175/1520-0493(1986)114⟨2488:teghtd⟩2.0.co;2

Mori, M., Kosaka, Y., Taguchi, B., Tokinaga, H., Tatebe, H., & Nakamura, H. (2024). Northern hemisphere winter atmospheric teleconnections are intensified by extratropical ocean-atmosphere coupling. *Communications Earth amp; Environment*, *5*(1), 124. https://doi.org/10.1038/s43247-024-01282-1

Müller, W. A., & Roeckner, E. (2008). Enso teleconnections in projections of future climate in echam5/mpi-om. *Climate Dynamics*, *31*(5), 533–549. https://doi.org/10.1007/s00382-007-0357-3

O'Reilly, C. H. (2018). Interdecadal variability of the enso teleconnection to the wintertime north pacific. *Climate Dynamics*, *51*(9–10), 3333–3350. https://doi.org/10.1007/s00382-018-4081-y

Paek, H., Yu, J., & Qian, C. (2017). Why were the 2015/2016 and 1997/1998 extreme el niños different? *Geophysical Research Letters*, *44*(4), 1848–1856. https://doi.org/10.1002/2016gl071515

Peng, P., & Kumar, A. (2005). A large ensemble analysis of the influence of tropical ssts on seasonal atmospheric variability. *Journal of Climate*, *18*(7), 1068–1085. https://doi.org/10.1175/jcli-3314.1

Planton, Y. Y., Guilyardi, E., Wittenberg, A. T., Lee, J., Gleckler, P. J., Bayr, T., et al. (2021). Evaluating climate models with the clivar 2020 enso metrics package. *Bulletin of the American Meteorological Society*, *102*(2), E193–E217. https://doi.org/10.1175/bams-d-19-0337.1

Power, S., Lengaigne, M., Capotondi, A., Khodri, M., Vialard, J., Jebri, B., et al. (2021). Decadal climate variability in the tropical pacific: Characteristics, causes, predictability, and prospects. *Science*, *374*(6563). https://doi.org/10.1126/science.aay9165

Rasmusson, E. M., & Carpenter, T. H. (1982). Variations in tropical sea surface temperature and surface wind fields associated with the southern oscillation/el niño. *Monthly Weather Review*, *110*(5), 354–384. https://doi.org/10.1175/1520-0493(1982)110⟨0354:vitsst⟩2.0.co;2

Rayner, N. A., Parker, D. E., Horton, E. B., Folland, C. K., Alexander, L. V., Rowell, D. P., et al. (2003). Global analyses of sea surface temperature, sea ice, and night marine air temperature since the late nineteenth century. *Journal of Geophysical Research*, *108*(D14). https://doi.org/10.1029/2002jd002670

Ren, H.-L., & Jin, F.-F. (2011). Niño indices for two types of ENSO. *Geophysical Research Letters*, *38*(4). https://doi.org/10.1029/2010gl046031

Roehrig, R., Beau, I., Saint-Martin, D., Alias, A., Decharme, B., Guérémy, J.-F., et al. (2020). The CNRM global atmosphere model ARPEGE-climat 6.3: Description and evaluation. *Journal of Advances in Modeling Earth Systems*, *12*(7). https://doi.org/10.1029/2020ms002075

Ropelewski, C. F., & Halpert, M. S. (1986). North american precipitation and temperature patterns associated with the el niño/southern oscillation (ENSO). *Monthly Weather Review*, *114*(12), 2352–2362. https://doi.org/10.1175/1520-0493(1986)114⟨2352:napatp⟩2.0.co;2

Sardeshmukh, P. D., Compo, G. P., & Penland, C. (2000). Changes of probability associated with el niño. *Journal of Climate*, *13*(24), 4268–4286. https://doi.org/10.1175/1520-0442(2000)013⟨4268:copawe⟩2.0.co;2

Seager, R., Hoerling, M., Schubert, S., Wang, H., Lyon, B., Kumar, A., et al. (2015). Causes of the 2011–14 California drought. *Journal of Climate*, *28*(18), 6997–7024. https://doi.org/10.1175/jcli-d-14-00860.1

Shin, N.-Y., Kug, J.-S., Stuecker, M. F., Jin, F.-F., Timmermann, A., & Kim, G.-I. (2022). More frequent central pacific el niño and stronger eastern pacific el niño in a warmer climate. *npj Climate and Atmospheric Science*, *5*(1), 101. https://doi.org/10.1038/s41612-022-00324-9

Srinivas, G., Vialard, J., Liu, F., Voldoire, A., Izumo, T., Guilyardi, E., & Lengaigne, M. (2024). Dominant contribution of atmospheric non-linearities to enso asymmetry and extreme el niño events. *Scientific Reports*, *14*(1), 8122. https://doi.org/10.1038/s41598-024-58803-3

Straus, D. M., & Shukla, J. (2000). Distinguishing between the sst-forced variability and internal variability in mid latitudes: Analysis of observations and gcm simulations. *Quarterly Journal of the Royal Meteorological Society*, *126*(567), 2323–2350. https://doi.org/10.1002/qj.49712656716

Straus, D. M., & Shukla, J. (2002). Does enso force the pna? *Journal of Climate*, *15*(17), 2340–2358. https://doi.org/10.1175/1520-0442(2002)015⟨2340:deftp⟩2.0.co;2

Takahashi, K., Montecinos, A., Goubanova, K., & Dewitte, B. (2011). ENSO regimes: Reinterpreting the canonical and modoki el niño. *Geophysical Research Letters*, *38*(10). https://doi.org/10.1029/2011gl047364

Taschetto, A. S., Ummenhofer, C. C., Stuecker, M. F., Dommenget, D., Ashok, K., Rodrigues, R. R., & Yeh, S.-W. (2020). ENSO atmospheric teleconnections. *Wiley*, 309–335. https://doi.org/10.1002/9781119548164.ch14

Taylor, K. E. (2001). Summarizing multiple aspects of model performance in a single diagram. *Journal of Geophysical Research*, *106*(D7), 7183–7192. https://doi.org/10.1029/2000jd900719

Timmermann, A., An, S.-I., Kug, J.-S., Jin, F.-F., Cai, W., Capotondi, A., et al. (2018). El niño–southern oscillation complexity. *Nature*, *559*(7715), 535–545. https://doi.org/10.1038/s41586-018-0252-6

Trenberth, K. E. (2019). The climate data guide: Nino sst indices (nino 1+2, 3, 3.4, 4; oni and tni). *National Center for Atmospheric Research Staff*, Retrieved from https://climatedataguide.ucar.edu/climate-data/nino-sst-indices-nino-12-3-34-4-oni-and-tni

Wallace, J. M., & Gutzler, D. S. (1981). Teleconnections in the geopotential height field during the northern hemisphere winter. *Monthly Weather Review*, *109*(4), 784–812. https://doi.org/10.1175/1520-0493(1981)109⟨0784:titghf⟩2.0.co;2

Xiang, B., Zhao, M., Held, I. M., & Golaz, J. (2017). Predicting the severity of spurious "double itcz" problem in cmip5 coupled models from amip simulations. *Geophysical Research Letters*, *44*(3), 1520–1527. https://doi.org/10.1002/2016gl071992

Xie, S.-P., Deser, C., Vecchi, G. A., Ma, J., Teng, H., & Wittenberg, A. T. (2010). Global warming pattern formation: Sea surface temperature and rainfall. *Journal of Climate*, *23*(4), 966–986. https://doi.org/10.1175/2009jcli3329.1

Yu, B., Zhang, X., Lin, H., & Yu, J.-Y. (2015). Comparison of wintertime north american climate impacts associated with multiple enso indices. *Atmosphere-Ocean*, *53*(4), 426–445. https://doi.org/10.1080/07055900.2015.1079697

Yu, J., Zou, Y., Kim, S. T., & Lee, T. (2012). The changing impact of el niño on us winter temperatures. *Geophysical Research Letters*, *39*(15). https://doi.org/10.1029/2012gl052483

Zhang, H., Xie, S., Seager, R., & Zhao, S. (2024). Dynamical constraint on precipitation biases over the indo-pacific region during boreal summer in amip6 models. *Geophysical Research Letters*, *51*(6). https://doi.org/10.1029/2023gl107181

Zhou, Z.-Q., Xie, S.-P., Zheng, X.-T., Liu, Q., & Wang, H. (2014). Global warming–induced changes in el niño teleconnections over the north pacific and north America. *Journal of Climate*, *27*(24), 9050–9064. https://doi.org/10.1175/jcli-d-14-00254.1